 doi:10.20944/preprints202210.0017.v1

Research Article

Nonlinear modeling of RC substandard beam-column joints for building response analysis in support of seismic risk assessment and loss estimation

Naveed Ahmad[1,*], Muhammad Rizwan[2], Babar Ilyas[3], Sida Hussain[3], Muhammad Usman Khan[4], Hamna Shakeel[3], Muhammad Ejaz Ahmad[3]

1 Department of Civil and Environmental Engineering, Stanford University, Stanford 94305, CA, USA.
2 Department of Civil Engineering, SUIT Peshawar, KP 25000, Pakistan.
3 Department of Civil Engineering, UET Peshawar, KP 25000, Pakistan.
4 National University of Sciences and Technology (NUST), Islamabad, Pakistan.
* Correspondence: drnaveed@stanford.edu

Abstract: The paper discusses how joint damage and deterioration affect the seismic response of existing reinforced concrete frames with sub-standard beam-column joints. The available simplified modeling techniques are critically reviewed to propose a robust, yet computationally efficient technique for simulating the nonlinear behavior of substandard beam-column joints. Improvements over the existing models include simulation of the cyclic deterioration of joint stiffness and strength as well as pinching in the hysteretic response, implemented considering a deteriorating hysteretic rule. A fibre-section forced-based inelastic beam-column element is developed; considering improved material models and fixed-end rotation due to bond failure, rebars-slip and inelastic extension, to simulate the deteriorating cyclic behavior of existing pre-cracked beam-column members. For the assessment of frames with substandard exterior beam-column joints, a nonlinear model for the exterior joint is developed and validated through a full-scale quasi-static cyclic test performed on a substandard T-joint connection. The proposed model allows considering structural performance in risk assessment while accounting for true inelastic mechanisms at the joints.

Keywords: beam-column joint; fibre-based section modeling; joint shear hinge; substandard beam-column joints; stiffness and strength deterioration; reinforced concrete; seismic vulnerability; risk

1. Introduction

A beam-column joint in the reinforced concrete moment-resisting frame is a most critical component; it experiences high axial and vertical and horizontal shear stresses during earthquakes and its behavior has a significant influence on the building seismic response. If not adequate, joint shear failure can result. However, if a joint is assumed to be stiff throughout the analysis during the assessment process, this may be overlooked. The shear failure of the beam-column joint almost often has a brittle character, which does not provide an adequate level of structural performance, particularly under extreme seismic actions (Moehle and Mahin, 1991). There have been several reports of catastrophic building collapses during strong earthquakes (Figure 1), which have been linked to beam-column joint failure, including those that occurred in the 1999 earthquakes in Chi-Chi, Taiwan, and Izmit, Turkey, and in the 1994 Northridge earthquake in California, USA (EERI, 1994). Therefore, it is crucial to comprehend joint behavior in the nonlinear building response analysis in order to make an informed judgment regarding the evaluation of building damages.

Over the past several decades, a number of studies have focused on understanding how beam-column joints respond to seismic actions (Aycardi *et al*., 1994; Beres *et al*., 1996; Gautam *et al*., 2021; Ahmad *et al*., 2019; Rizwan *et al*., 2018). Moreover, several international

Preprints (www.preprints.org) | NOT PEER-REVIEWED | Posted: 4 October 2022 doi:10.20944/preprints202210.0017.v1

seismic codes of practice have undergone repeated improvements to put the findings into practice. The most recent ACI joint design recommendations (ACI-352-R02) account for inelastic deformation in the joint panel. The present joint design procedures and detailing provisions offer resistance to the gravity loads, seismic actions, and the interaction of multidirectional forces applied to the joint from surrounding frame elements. To ensure an improved cycle behavior and a minimum plastic deformation capacity, sufficient development length and confinement in the joint panel are provided.

Recent research on the quantification of seismic risk of existing reinforced concrete structures has focused on frames with substandard beam-column joints that are prevailing in most seismically active countries. This paper focuses on comprehending the primary mechanism influencing the seismic nonlinear response of beam-column connections and presents a simplified nonlinear numerical modeling technique, which is crucial for assessing the seismic building's response. With particular reference to bond failure and rebar slip (resulting in member fixed-end rotation) and joint shear strength deterioration, this research studied the effects of exterior joint nonlinear behavior and underlines the crucial factors that influence structural performance, which is fundamental for risk assessment and repair cost estimation.

Figure 1. Partial collapse of buildings documented during large damaging earthquakes: from left to right: 1999 Izmit earthquake in Turkey, 1999 Chi-Chi earthquake in Taiwan, and 1994 Northridge earthquake in the USA.

2. Critical Review of Simplified Nonlinear Modeling Techniques for RC Beam-Column Joints

Modeling frames with weaker joints for nonlinear seismic analysis has been attempted using different simplified techniques (Figure 2). These are briefly reviewed here to serve as a basis for the development of a more robust, yet simplified and computationally efficient analytical model of reinforced concrete frames that incorporates both shear and bond mechanisms behavior of beam-column joints and fixed-end rotation of connecting members, and that can be used for both local and global damage evaluation.

The flexural strengths of the beams and columns framing the joint were decreased by Kunnath *et al*. (1995) to take into consideration the insufficient joint shear strength capacity. However, such implicit models are incapable to account for the additional deformation resulting from the joint bond mechanism and the pinching effects on frame hysteretic response due to joint shear stiffness and strength deterioration. El-Metwally *et al*. (1988) used a zero-length spring with nonlinear behavior to model the shear deformation of the joint panel. Through the use of rotational springs, Biddah and Ghobarah (1999) modeled joint shear and bond-slip deformations. Later, Ghobarah and Biddah (1999) utilized the model to demonstrate that joint deformations led to greater flexibility and drifts under seismic actions. These models, however, were unable to accurately simulate joint shear deterioration. Alath and Kunnath (1995) used a rotational spring model to explicitly simulate the joint shear deformation, with deteriorating hysteresis being established empirically but this has the drawback that it must repeatedly be calibrated for various beam-column joints. Pampanin *et al*. (2003) proposed a similar simplified model with a moment-rotational spring and deteriorating hysteretic response. The spring's properties were

Preprints (www.preprints.org) | NOT PEER-REVIEWED | Posted: 4 October 2022 doi:10.20944/preprints202210.0017.v1

directly deduced from the corresponding principal tensile stress vs. shear deformation curve, which in turn was based on a large experimental database (Priestley *et al*., 1997), using the equilibrium consideration. This, however, falls short of accurately simulating the deterioration of joint shear strength. Sharma *et al*. (2011) improved upon this approach by including additional shear springs in the joint panel to account for the panel's shear deformation and to take strength degradation into consideration. The model still does not adequately account for stiffness and strength deterioration, which is essential for sub-standard beam-column joints. The same is true for the method proposed by Khan *et al*., (2020).

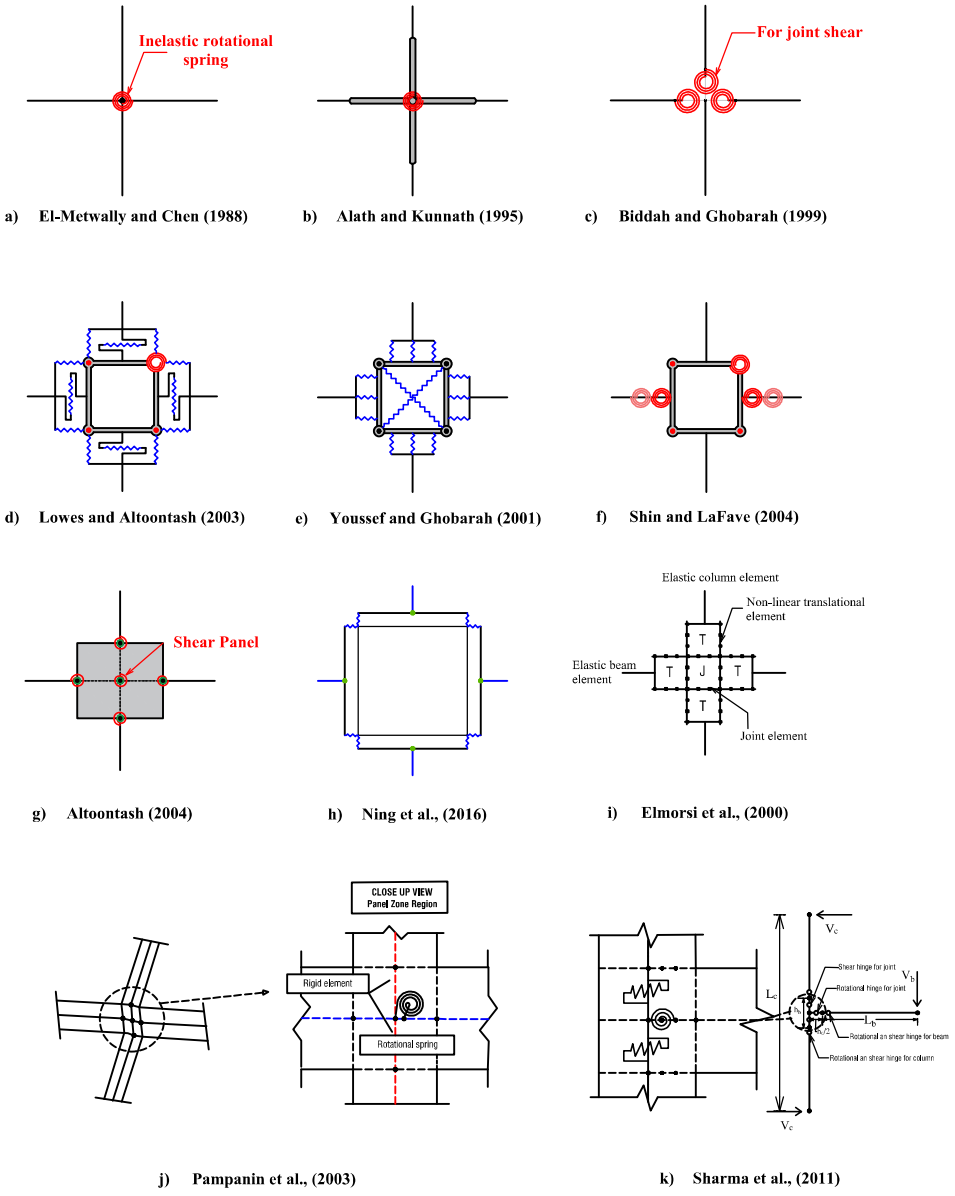

Figure 2. Existing simplified analytical models for nonlinear modeling of reinforced concrete beam-column joint

Adding an extra infinitely stiff bar attached to the plastic beam sub-element with plastic hinges at the ends, Filippou *et al*. (1983) and Filippou and Issa (1988) developed an

 doi:10.20944/preprints202210.0017.v1

explicit model to simulate the fixed-end rotations and the sliding due to shear at the beam-column interface. Although promising in simulating the rotational and bending-moment resistance of the beam-column joint, it is unable to simulate the joint shear deterioration and the pinching that results in the hysteretic response of the frame.

Youssef and Ghobarrah (2001) developed a 14-spring element assembly for a beam-column joint that included two diagonal springs to simulate joint shear deformation and twelve translational springs placed at the panel zone interface to represent the inelastic mechanisms of connecting beam/column members. It models the shear strength deterioration but implicitly considers rebar slip and rebar inelasticity. A model developed by Ning *et al*., (2016) included one spring for the panel zone and eight springs for the rebar-slip, and employing the Bouc-Wen- Baber-Noori model (Baber and Noori, 1985) to simulate the hysteretic behavior of the panel zone. The model, however, is unable to truly replicate the cyclic strength and stiffness deterioration that occurs often at substandard beam-column joints.

Another model suggested by Elmorsi *et al*. (2000) involved idealizing beams and columns as elastic elements connected to the joint by the intervention of non-linear transitional elements, modeled using other elements made up of 12 parts. The model takes into account the effects of bond-slip and joint shear deformations and can simulate the deterioration of bonds and eventual pullout of reinforcing bars during extreme cyclic loads. The model is clumsy and computationally expensive when a large number of analyses are required for building performance assessment.

A 4-node 12-degree-of-freedom joint panel was proposed by Lowes and Altoontash (2003) that constitutes a panel zone component with a zero-length rotational spring simulating the shear deformation of the joint with additional four zero-length shear springs for simulating the interface-shear deformations. A total of eight zero-length translational springs were included to simulate the bar slip. The panel zone's shear stress-strain relationships were determined using the modified compression field theory MCFT (Vecchio and Collins, 1986). Later, Lowes *et al*. (2004) attempted to simulate the interface-shear based on experimental data; this work anticipated an interface-shear response that was stiff and elastic. Moreover, specimens with at least a minimal degree of transverse reinforcement in the panel zone were included in the experimental data for validation, which is compatible with the model's intended usage. However, they did not include joints that lack transverse reinforcement, therefore, it cannot be used to analyze weaker joints of frames that lack transverse reinforcement. The model proposed by Lowes and Altoontash (2003) was further simplified by Altoontash (2004) by adding four rotational springs to member ends to simulate the bar-slip phenomenon and a rotational spring that was defined in the panel zone to simulate the shear distortion of the joint. However, it is still insufficient for the analysis of joints lacking transverse reinforcement and members exhibiting large fixed-end rotation.

Shin and LaFave (2003) proposed an analytical model for a beam-column joint where the joint panel was made up of stiff elements along the panel zone's edges and three parallel rotational springs provided in one of the four hinges connecting the parallelogram's sides. The MCFT was used to anticipate the joint shear stress-strain response envelope while the cyclic response was calibrated using experimental data. Two rotating springs (in series) are positioned at the interfaces between the beam and the joint to separately simulate the member-end rotations produced by the bond-slip behavior of the longitudinal beam reinforcement and plastic hinge rotations induced by the inelastic behavior of the beam. The model is robust in simulating joint shear deterioration, bond mechanisms, and fixed-end rotation.

The assessment of beam-column joints without transverse reinforcement presents some difficulties for most of the modeling techniques discussed above. Some of these, for example, are computationally inefficient and need simplification in order to be implemented in the available finite element-based programs for large analysis, while others are only appropriate for joints that have been seismically designed and detailed, and less accurate when applied to substandard beam-column joints with pre-existing cracks in the

Preprints (www.preprints.org) | NOT PEER-REVIEWED | Posted: 4 October 2022 doi:10.20944/preprints202210.0017.v1

structural members. The goal of the present study is to propose a more robust modeling technique that would still be computationally efficient and capable to model the deterioration of stiffness and strength common to existing frames with substandard beam-column joints subjected to cyclic loading.

3. Proposed Nonlinear Modeling Technique for RC Substandard Beam-Column Joints

3.1. Mechanics of Exterior Beam-Column Joints

Figure 3 illustrates the internal forces and reactions acting on a reinforced concrete exterior beam-column joint under seismic actions. If it is assumed that the points of zero bending moment are located at the half-height of the column and the half-span of the beam, respectively, then it can be assumed that column shear $V_a = V_c$ and column moment $M_a = M_c$. The reversal of the moment across the joint necessitates that the reinforcement of the beam is in compression on one side and at a tensile yield on the other. The internal horizontal tension T_b, compression C_b, and vertical beam shear V_b forces introduced by the beam to the column are shown. Making the approximations that $C_b = T_b$, the require horizontal column shear force V_{jh} across the joint region based on the equilibrium of free body is:

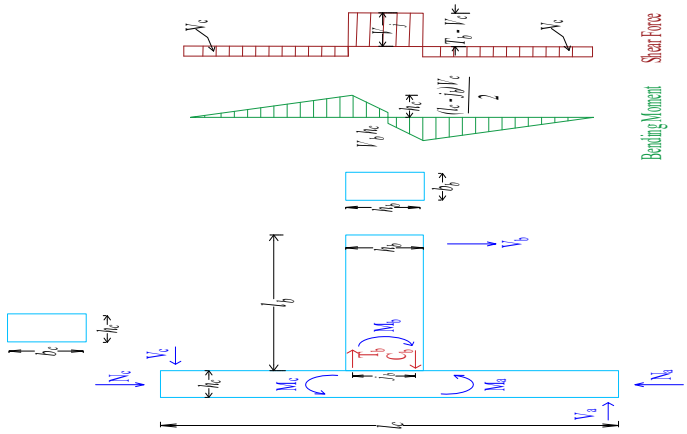

Figure 3. Internal forces and reactions in beam-column joints under lateral loads.

$$V_{jh} = T_b - V_c \tag{1}$$

$$T_b = \frac{M_b}{j_b} \tag{2}$$

$$T_b = \frac{V_b l_b}{j_b} \tag{3}$$

Where M_b is the beam moment, l_b is the length of beam, h_c is the depth of column, and j_b is the internal level arm between the tensile force and the centroid of the compressive forces. This can be determined by moment-curvature analysis of the beam or approximated as follows:

$$j_b = d_b - d'_b \tag{4}$$

where d_b is the effective depth of beam and d'_b is the effective cover to compression reinforcement. The column top load V_c can be calculated corresponding to the beam moment extended linearly to the centerline of the joint:

$$V_c = \frac{V_b(l_b + 0.5h_c)}{l_c} \tag{5}$$

where l_c is the length of column. Substituting Eq. (5) and (3) in Eq. (1), the following expression is obtained for horizontal joint shear force V_{jh}:

Preprints (www.preprints.org) | NOT PEER-REVIEWED | Posted: 4 October 2022 doi:10.20944/preprints202210.0017.v1

$$V_{jh} = V_b \left(\frac{l_b}{j_b} - \frac{l_b + 0.5h_c}{l_c} \right) \tag{6}$$

The resulting horizontal and vertical shear stress, v_{jh} and v_{jv}, at the mid-depth of the joint core is:

$$v_{jh} = v_{jv} = \frac{V_{jh}}{h_c' b_c'} \tag{7}$$

where h'_c and b'_c are the length and width of joint core. The joint region is subjected to horizontal and vertical shear stresses that are typically many times greater than those in the adjacent beams and columns. These are equal depends on the joint aspect ratio α:

$$\alpha = \frac{V_{jv}}{V_{jh}} = \frac{h_b}{h_c} \tag{8}$$

Moreover, the axial compressive stress f_a at the mid-depth of the joint core due to vertical force N_c acting on the column is:

$$f_a = \frac{N_c}{h_c' b_c'} \tag{9}$$

The joint shear and axial stresses lead to the diagonal compression and tension principal stresses in the joint core. The principal compression stress f_c and tension stress f_t at mid-depth of the joint core can be found using Mohr's circle:

$$f_{t,c} = \frac{f_a}{2} \pm \sqrt{\left(\frac{f_a}{2}\right)^2 + v_{jh}^2} \tag{10}$$

Once the joint core develops diagonal tension cracks, the joint core's diagonal compression strut and truss mechanism, consisting of a concrete diagonal compression field and horizontal and vertical reinforcement, transfers the beam and column forces across the joint core (Figure 4). A beam-column joint may experience various damage or failure mechanisms as a result of the adopted structural detailing. It has been demonstrated that the use of poor-quality concrete, a lack of transverse reinforcement in the joint region, and inadequate anchoring details all constitute potential causes of a highly brittle failure mechanism. Because the shear and bond mechanisms that control the joint response have poor hysteretic properties, as a result, the joint's rotational resistance degrades rapidly (Park, 2002; Paulay and Priestley, 1992).

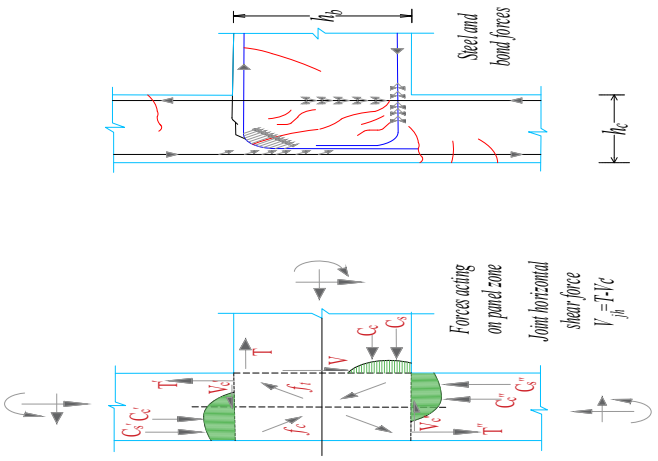

Figure 4. Principal stresses developed in joint core, and the resulting cracking of joint, bond and bearing forces developed after the initiation of diagonal cracks.

3.2. Modeling of Joint Shear Panel

Preprints (www.preprints.org) | NOT PEER-REVIEWED | Posted: 4 October 2022 doi:10.20944/preprints202210.0017.v1

Figure 5 illustrates the proposed analytical model for a substandard RC external beam-column joint subjected to seismic actions. The beam elements and the column elements are located at the beam mid-depth and the column mid-depth, respectively. The assembly is envisaged, as the same is tested experimentally. The joint panel distortion is modeled by four rigid link elements arranged along the edges of the joint panel and one nonlinear rotational spring is incorporated in one of the four hinges connecting the adjacent rigid elements. The failure of an exterior joint is primarily related to the principal tensile stress developed in the joint core.

The critical parameter is the principal tension stress within the joint core, joint cracking begins at a stress of $0.29(f_c')^{0.5}$ MPa. In the case of exterior joints lacking transverse reinforcement, the experimental data support the highest principal tension stress of $0.42(f_c')^{0.5}$. Joint shear strength deterioration is governed by the gradual reduction of the effective joint principal tension stress (Priestley *et al*., 1997; Calvi *et al*., 2002). The principal tensile stress vs. shear deformation envelope curve illustrated in Figure 6(a) is used to directly deduce the moment-rotation properties of the joint spring based on the equilibrium considerations. The nonlinear rotational spring at the joint is assigned a multilinear deteriorating hysteretic rule (Ibarra *et al*., 2005) to simulate the joint stiffness and strength deterioration and pinching in the hysteretic response (Figure 6(b)), which is crucial for the shear failure of substandard beam-column joints.

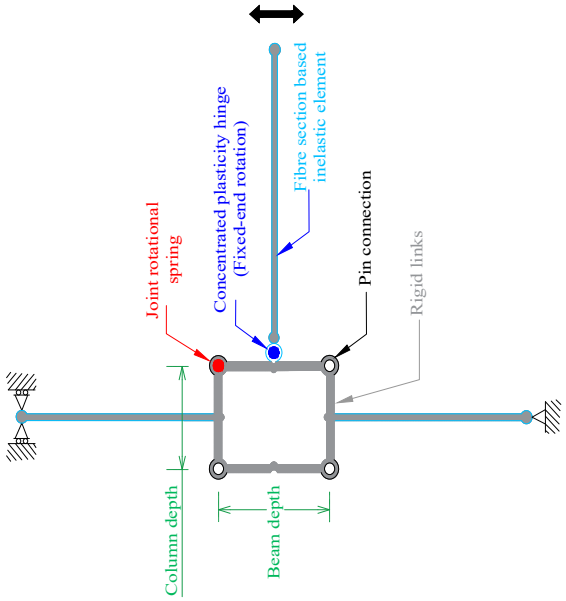

Figure 5. Nonlinear FE-based numerical model for exterior beam-column joint.

3.3 Modeling of Beam-Column Connecting Members

The flexibility-based element formulation, such as that developed by Spacone *et al*. (1996a), which is an extension of the Ciampi and Carlesimo (1986) proposed consistent flexibility-based method for formulating frame members, is established using the framework of the mixed method formulation (Spacone *et al.*, 1996b). The element formulation strictly satisfies the equilibrium of bending moments and axial force along the element using force interpolation functions rather than displacement interpolation functions. The element state determination relies on a nonlinear iterative method based on residual deformations (Spacone *et al.*, 1996b) that continuously maintains equilibrium within the element and finally converges to a state that satisfies the element constitutive relation within a set tolerance.

Preprints (www.preprints.org) | NOT PEER-REVIEWED | Posted: 4 October 2022 doi:10.20944/preprints202210.0017.v1

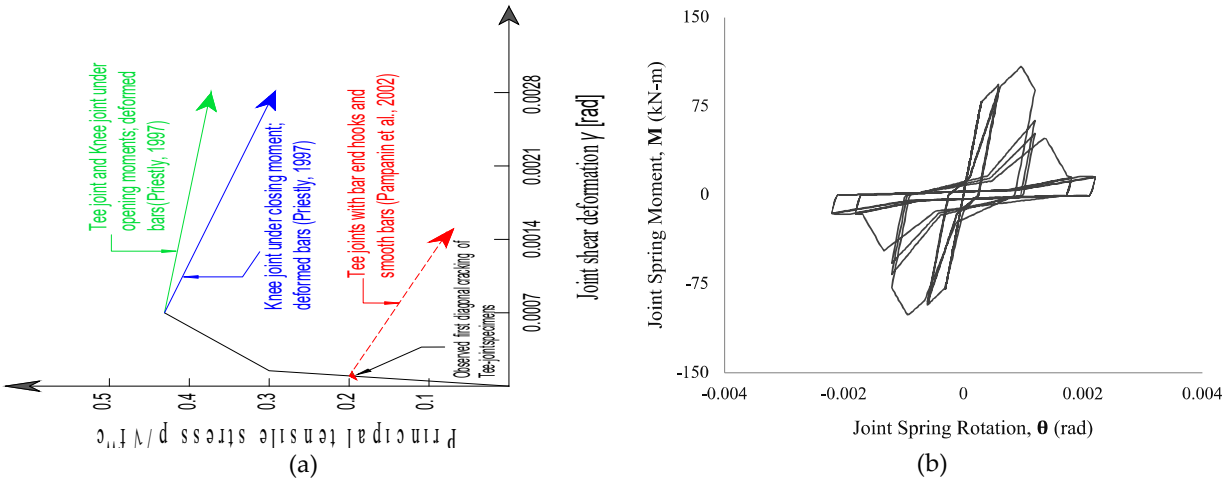

Figure 6. (a) Joint shear strength degradation model for exterior and corner joints (Priestley *et al.*, 1997). (b) hysteretic rule used to model joint stiffness and strength deterioration.

The element stiffness matrix is obtained by inverting the element flexibility matrix. The use of improved material models to simulate the element's deteriorating hysteretic response owing to pre-existing cracks in the member, the rigid body fixed-end rotation due to rebars slip and inelastic extension, and geometric nonlinearity are improvements in the present model over the original formulation of Spacone *et al.* (1996a). This solution technique is especially well suited for the study of the highly nonlinear deteriorating hysteretic behavior of the substandard reinforced concrete elements.

The fiber-based approach, in which each fiber is assigned a uniaxial stress-strain relationship, is used by the frame beam-column element to simulate the cross-section behavior. The nonlinear uniaxial stress-strain response of the individual fibers into which the section has been divided is then integrated to provide the sectional stress-strain state. Because the material constitutive models already specify hysteretic response, a fiber section-based element has the advantage of not requiring prior moment-curvature analysis and calibration. Moreover, it directly simulates the stiffness and strength interactions between an axial load and a bending moment as well as the interactions between flexural strength in orthogonal directions. The discrete number of the controlling sections along the element that are used for the numerical integration is the only approximation in this formulation, and it doesn't actually impose any restrictions on the displacement field of the element, this formulation is always "exact": regardless of the degree of inelasticity, the force field is always exact. To prevent under-integration, a minimum of 3 Gauss-Lobatto integration sections are necessary and in general 5-7 integration points (IPs) are utilized (Papadrakakis *et al.*, 2008; Calabrese *et al.*, 2010) to adequately model the spread of inelasticity.

3.3.1 Beam-Column Element Formulation

Model assumptions:

- Beam-column element in local reference system x, y, z (Figure 7(a))
- A discrete number of cross sections placed at control points of the numerical integration
- Beam-column member geometry is linear
- Plane sections remain plane and are normal to the longitudinal axis throughout the deformation history
- Strains and stresses act parallel to the longitudinal axis
- Member behavior in torsion is linearly elastic and uncoupled from flexure and axial response

Preprints (www.preprints.org) | NOT PEER-REVIEWED | Posted: 4 October 2022 doi:10.20944/preprints202210.0017.v1

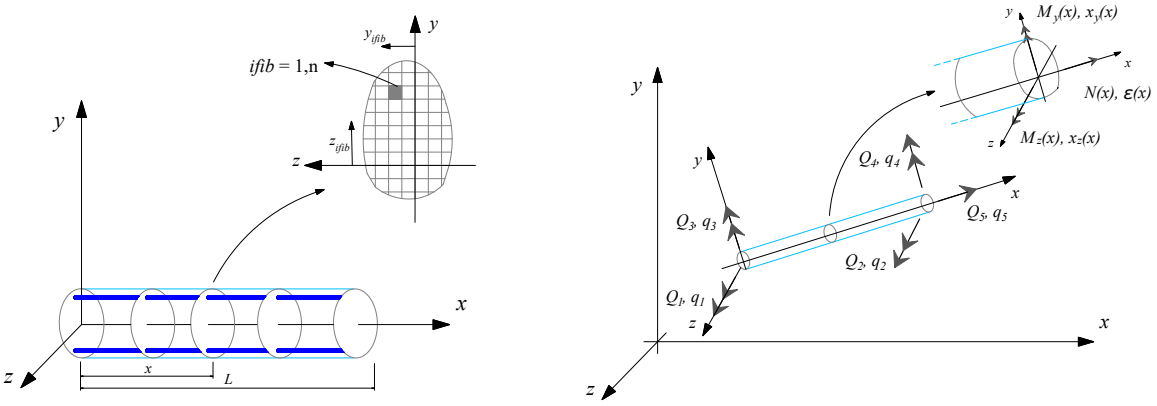

(a) Member local reference system (b) Forces and deformation at section and member level

Figure 7. Beam element in the local reference system: subdivision of cross-section into fibres

Vectors of element forces and deformations and the corresponding section forces and deformations are given below:

$$Q = \{Q_1, Q_2, Q_3, Q_4\}^T \tag{11}$$

$$q = \{q_1, q_2, q_3, q_4\}^T \tag{12}$$

$$D(x) = \{M_z(x), M_y(x), N(x)\}^T \tag{13}$$

$$d(x) = \{X_z(x), X_y(x), \bar{\varepsilon}(x)\}^T \tag{14}$$

where Q is the element force vector, q is the element deformation vector, $D(x)$ is the section force vector, and $d(x)$ is the section deformation vector, $X(x)$ is the section curvature about the reference axis, and $\bar{\varepsilon}(x)$ is the axial strain at the reference axis. With the use of a simple geometric transformation matrix, the fibre strains are related to section deformations. The section forces and deformations are related to element forces and deformations using the force and deformation interpolation functions:

$$\Delta d(x) = a(x)\Delta q \tag{15}$$

$$\Delta D(x) = b(x)\Delta Q \tag{16}$$

where matrix $a(x)$ is the deformation interpolation function and matrix $b(x)$ is the force interpolation function, Δ is the increments of the corresponding quantities. Linearization of the incremental section constitutive relation is according to the Equation (17):

$$\Delta d^j(x) = f^{j-1}(x)\Delta D^j(x) + r^{j-1}(x) \tag{17}$$

where $f^{j-1}(x)$ is the section flexibility and $r^{j-1}(x)$ is the residual deformations from the previous iteration. The residual deformation $r^{j-1}(x)$ is the linear approximation to the deformation error that results from linearizing the section force-deformation relation. Equation (17) may be presented in the integral form as given:

$$\int_0^L \delta D^T(x)\left[\Delta d^j(x) - f^{j-1}(x)\Delta D^j(x) - r^{j-1}(x)\right]d_x \tag{18}$$

Substituting Equation (15) and (16) in Equation (18) gives:

Preprints (www.preprints.org) | NOT PEER-REVIEWED | Posted: 4 October 2022 doi:10.20944/preprints202210.0017.v1

$$T\Delta q^j - F^{j-1}\Delta Q^j - s^{j-1} = 0 \tag{19}$$

where T is the matrix dependent on the interpolation functions, F is the element flexibility matrix, and s is the element residual deformation vector given as follows:

$$T = \int_0^L b^T(x)a(x)d_x \tag{20}$$

$$F = \int_0^L b^T(x)f(x)b(x)d_x \tag{21}$$

$$s = \int_0^L b^T(x)r(x)d_x \tag{22}$$

Furthermore, the virtual displacement principle is used to obtain the integral form of the equilibrium equation:

$$\int_0^L \delta d^T(x)\left[D^{j-1}(x) + \Delta D^j(x)\right]d_x = \delta q^T Q^j \tag{23}$$

where $D^{j-1}(x) + D^j$ is the new internal force distribution and Q^j is the corresponding vector of nodal forces in equilibrium. Substituting Equations (15) and (16) in Equation (23), results in the following matrix expression, which is equivalent of the integral form of the element equilibrium equations:

$$T^T Q^{j-1} + T^T \Delta Q^j = Q^j \tag{24}$$

The combination of Equation 19 and 24 results in the following expression:

$$\begin{bmatrix} -F^{j-1} & T \\ T^T & 0 \end{bmatrix} = \begin{Bmatrix} \Delta Q^j \\ \Delta q^j \end{Bmatrix} = \begin{Bmatrix} s^{j-1} \\ Q^j - T^T Q^{j-1} \end{Bmatrix} \tag{25}$$

Solving the first equation for ΔQ^j and substituting it in the second equation results in the following expression:

$$T^T\left[F^{j-1}\right]^{-1}\left(T\Delta q^j - s^{j-1}\right) = Q^j - T^T Q^{j-1} \tag{26}$$

Assuming $T = I$, as peculiar to the proposed Bernoulli beam, where I is a 3x3 identity matrix, the above equation is simplified as:

$$\left[F^{j-1}\right]^{-1}\left(\Delta q^j - s^{j-1}\right) = \Delta Q^j \tag{27}$$

where ΔQ^j is the element force increment, $(\Delta q^j - s^{j-1})$ is the corresponding deformation increment including the residual deformation s^{j-1} that results from the linearization of the section's non-linear constitutive relations, and $[F^{j-1}]^{-1}$ is the element stiffness matrix obtained by inverting the flexibility matrix.

The element forces provide the most difficulty since they cannot be easily calculated from the section forces, even if the element stiffness matrix is obtained by inverting the element flexibility matrix. The procedure outlined in Spacone *et al*., (1996b) presents an iteration scheme at the element level that is similar to the Newton-Raphson method utilized for the structure level solution of the equilibrium equations. Force increments are applied to the structural degrees of freedom, and Newton-Raphson iterations are used to reduce the imbalanced forces down to acceptable levels at each load step. The structural level solution of these equations results in displacement increments at the end nodes of

Preprints (www.preprints.org) | NOT PEER-REVIEWED | Posted: 4 October 2022 doi:10.20944/preprints202210.0017.v1

each element. The algorithm's iterations during the element state determination phase intend to reduce the deformation residuals to levels that are acceptable. In step *i* of the Newton-Raphson algorithm at the structural degrees of freedom, Figure 8 illustrates the relationship between element and section state determination. The following describes the iteration scheme used to determine the incremental element forces:

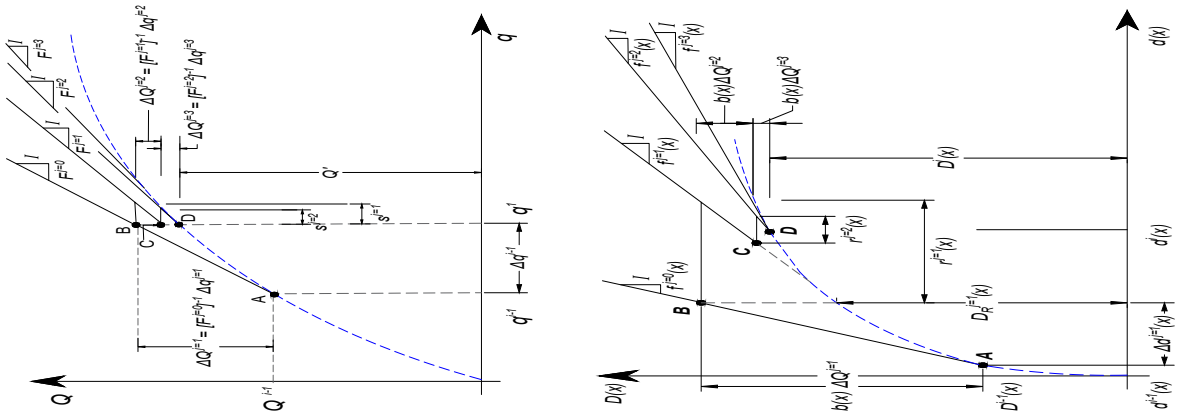

(a) Element state determination (b) Section state determination

Figure 8. Determination of element resisting forces Q^i corresponding to element deformations q^i using the element and state determination for a flexibility-based element.

At point A, $i = 1$ and $j = 0$:

element deformation $$q^i = q^{i-1} + \Delta q^i \tag{28}$$

iteration starts, $j = 1$

element force increment $$\Delta Q^{j=1} = [F^{j=0}]^{-1} \Delta q^{j=1} \tag{29}$$

initial element tangent stiffness matrix $$[F^{j=0}]^{-1} = [F^{i-1}]^{-1}$$

element deformation increment $$\Delta q^{j=1} = \Delta q^i$$

section deformation increment $$\Delta d^{j=1}(x) = f^{j=0}(x) \Delta D^{j=1}(x) \tag{30}$$

$$f^{j=0}(x) = f^{i-1}(x)$$

$$\Delta D^{j=1}(x) = b(x) \Delta Q^{j=1}$$

section deformation $$d^{j=1}(x) = d^{j-1}(x) + \Delta d^{j=1}(x) \tag{31}$$

Equation (31) provides the updated section deformation that corresponds to point B in Figure 8; this updated section deformation is used as the basis to determine the section stiffness and resisting forces. Assuming that plane sections remain plane and normal to the longitudinal axis, it is straightforward to determine the strain distribution in a section. The stress and tangent modulus of the section is obtained using the constitutive equations of the steel and concrete fibers, which are integrated over the cross-sectional area to determine the section's resisting forces and tangent stiffness matrix.

section stiffness matrix $$k^{j=1}(x) = \int_{A(x)} I^T(y,z) E(x,y,z) I(y,z) dA \tag{32}$$

section resisting forces $$D_R^{j=1}(x) = \int_{A(x)} I^T(y,z) \sigma(x,y,z) dA \tag{33}$$

geometric vector $$I(y,z) = \{-y\ z\ 1\}$$

Preprints (www.preprints.org) | NOT PEER-REVIEWED | Posted: 4 October 2022 doi:10.20944/preprints202210.0017.v1

The Gauss-Lobatto numerical integration scheme is used to solve Equations (32) and (33). The section stiffness is inverted to produce the flexibility matrix $f^{j=1}(x)$. The difference between the applied and resisting forces gives the unbalanced forces at the section.

unbalanced forces at the section $$D_U^{j=1}(x) = D^{j=1}(x) - D_R^{j=1}(x) \quad (34)$$

residual section deformations $$r^{j=1}(x) = f^{j=1}(x) D_U^{j=1}(x) \quad (35)$$

residual element deformations $$s^{j=1} = \int_0^L b^T(x) r^{j=1}(x) dx \quad (36)$$

second iteration, $j = 2$

updated element forces $$Q^{j=2} = Q^{j=1} + \Delta Q^{j=2} \quad (37)$$

compatibility corrective element forces $$\Delta Q^{j=2} = -\left[F^{j=1}\right]^{-1} s^{j=1}$$

updated section forces $$D^{j=2}(x) = D^{j=1}(x) + \Delta D^{j=2}(x) \quad (38)$$

updated section deformation $$d^{j=2}(x) = d^{j=1}(x) + \Delta d^{j=2}(x) \quad (39)$$

force increment applied at all IPs $$\Delta D^{j=2}(x) = b(x) \Delta Q^{j=2}$$

deformation increment induced at all IPs $$\Delta d^{j=2}(x) = r^{j=1}(x) + f^{j=1}(x) \Delta D^{j=2}(x)$$

$$r^{j=2}(x) = f^{j=2}(x) D_U^{j=2}(x) \quad (40)$$

At the completion of the second iteration, the state of the element and the sections corresponds to point C in Figure 8. The section flexibility matrices and section residual deformation vectors are determined at each control IPs. The new element flexibility matrix is obtained by integrating the section flexibility matrices in accordance with Equation (21). The residual section deformations are then integrated to yield the residual element deformations. The third and subsequent iterations adhere to this iteration scheme. When the specified element convergence criterion is satisfied, convergence is achieved. The measures of energy are used for the purpose (Taucer *et al*., 1991).

3.3.2 Material Models

The solution of equations (32) and (33) necessitates the definition of suitable material models since a numerical solution algorithm should include stress-strain relations for concrete and reinforcing rebars for computing the section resisting forces and stiffness matrix.

The Menegotto and Pinto (1973) nonlinear model, as updated by Filippou *et al*., (1983) to include isotropic strain hardening, has been used in the present study to characterize the stress-strain relation of the reinforcing steel. This is the most appealing since it has the best agreement with experimental data and is computationally efficient. The stress-strain model takes on the following form to describe a curved transition from a straight-line asymptote with slope E_0 to another asymptote with slope bE_0, and allowing a good representation of the Bauschinger effect:

$$\sigma^* = b\varepsilon^* + \frac{(1-b)\varepsilon^*}{[1 + (\varepsilon^*)^R]^{\frac{1}{R}}} \quad (41)$$

$$\sigma^* = \frac{(\sigma - \sigma_r)}{(\sigma_0 - \sigma_r)}$$

$$\varepsilon^* = \frac{(\varepsilon - \varepsilon_r)}{(\varepsilon_0 - \varepsilon_r)}$$

$$R^n = R_0 - \frac{a_1 \xi_p^n}{(a_2 + \xi_p^n)}$$

$$\xi_p^n = \varepsilon_r^n - \varepsilon_y^n$$

Preprints (www.preprints.org) | NOT PEER-REVIEWED | Posted: 4 October 2022 doi:10.20944/preprints202210.0017.v1

where σ^* and ε^* are the normalized stress and strain, σ_0 and ε_0 are the stress and strain at first yielding, b is strain hardening, σ_r and ε_r indicate the stress and the strain at the point of the last strain reversal with the stress of equal sign took place, R is the curvature parameter, R_0 is the value of R during the first loading, a_1 and a_2 are experimentally determined parameters, ξ_p^n is the plastic excursion at the current semicycle (Figure 9). Fragiadakis *et al*., (2007) provide more in-depth information on the model's numerical implementation that also takes into consideration the buckling of steel bars.

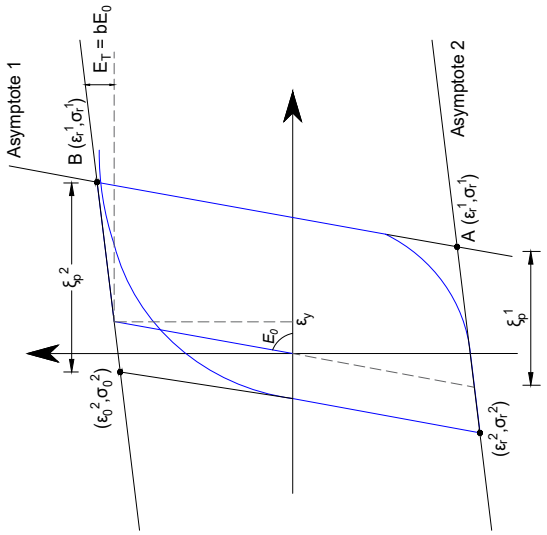

Figure 9. Stress-strain relationship of reinforcing steel material models used in inelastic beam-column members

In order to compute the concrete compressive forces, the cross-section can be divided into layers and the distribution of concrete strain is determined assuming a linear distribution of concrete strain increments and strain increment compatibility between steel and concrete. For this purpose, a nonlinear constant confinement concrete model (Figure 10), which is a uniaxial nonlinear model that is based on the constitutive relationship proposed by Mander *et al*. (1988) with modifications made by Martinez-Rueda and Elnashai (1997) for the purpose of maintaining numerical stability under large deformations, has been used to determine the stress in each layer. The ratio of the compressive stress of confined concrete to the unconfined concrete defines the constant confinement factor. Given the effective confined concrete core area A_e (mid-way through two consecutive stirrups) and area of concrete core A_{cc}, the effective confinement factor K_e is determined:

$$K_e = \frac{A_e}{A_{cc}} = \frac{A_e}{A_c(1-\rho_{cc})} \tag{42}$$

$$A_e = \left(b_c d_c - \sum_{i=1}^{n} \frac{(w_i')^2}{6}\right)\left(1 - \frac{s'}{2b_c}\right)\left(1 - \frac{s'}{2d_c}\right)$$

where ρ_{cc} is the ratio of area of longitudinal reinforcement to the area of core section, A_c is the area of the core of section enclosed by the center lines of the perimeter tie, b_c and d_c are the core dimensions to the centerlines of perimeter lateral tie, w_i' is the ith clear distance between adjacent longitudinal bars, s′ is the clear vertical spacing between lateral ties. Figure 11 illustrates a concrete model for both confined and unconfined concrete based on the stress-strain relation proposed by Mander *et al*. (1988), gives the longitudinal compressive concrete stress:

Preprints (www.preprints.org) | NOT PEER-REVIEWED | Posted: 4 October 2022 doi:10.20944/preprints202210.0017.v1

$$f_c = \frac{f'_{cc} x r}{r - 1 + x^r} \tag{43}$$
$$x = \frac{\varepsilon_c}{\varepsilon_{cc}}$$
$$\varepsilon_{cc} = \varepsilon_{co}\left[1 + 5\left(\frac{f'_{cc}}{f'_{co}} - 1\right)\right]$$
$$r = \frac{E_c}{E_c - E_{sec}}$$
$$E_{sec} = \frac{f'_{cc}}{\varepsilon_{cc}}$$
$$E_c = 5000\sqrt{f'_{co}} \quad \text{MPa}$$

The cover concrete has been designated as unconfined concrete, the stress-strain behavior of the segment of the falling branch in the area where $\varepsilon_c > 2\varepsilon_{co}$ is considered to be a straight line that reaches zero stress at the spalling strain ε_{sp}.

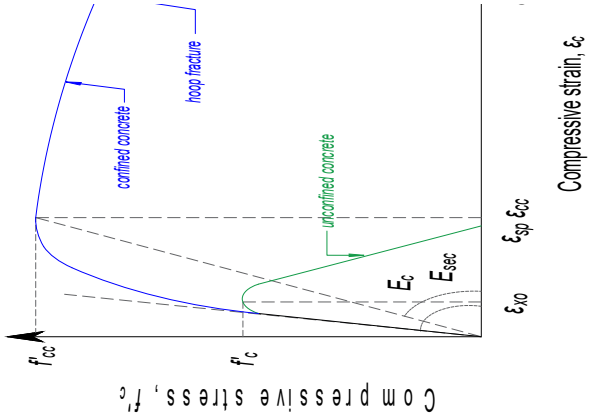

Figure 10. Stress-strain relationship of confined and unconfined concrete material models used in inelastic beam-column members

The confined compressive strength f'_{cc} is determined, assuming the confined concrete core is placed under triaxial compression with equal effective lateral confining forces f'_l from lateral ties:

$$f'_{cc} = f'_{co}\left(-1.254 + 2.254\sqrt{1 + \frac{7.94 f'_l}{f'_{co}}} - 2\frac{f'_l}{f'_{co}}\right) \tag{44}$$
$$f'_{lx} = K_e \rho_x f_{yh}$$
$$f'_{ly} = K_e \rho_y f_{yh}$$
$$\rho_x = \frac{A_{sx}}{s d_c}$$
$$\rho_y = \frac{A_{sy}}{s b_c}$$

where f_{yh} is the yield strength of the transverse reinforcement, A_{sx} and A_{sy} are the total area of transverse bars running in the x and y directions respectively, f'_{lx} and f'_{ly} the effective lateral confining stresses in the x and y directions respectively. In tension, a linear stress-strain relationship is assumed up to the tensile strength, provided the tensile strength has not been exceeded. However, it can be ignored for pre-cracked member with zero tensile strength. The cyclic loading stress-strain response is assumed to be enclosed by the monotonic loading stress-strain curve (Figure 10).

 doi:10.20944/preprints202210.0017.v1

When the transverse reinforcement confining the core fractures, it is regarded as the ultimate limit to confined concrete compression strain. This may be determined by comparing the increase in the strain-energy absorbed by the concrete over the value suitable for unconfined concrete to the strain-energy capacity of the confining steel. The following equation for the ultimate compression strain for confined concrete may be derived by assuming that the ultimate strain of the unconfined concrete is 0.004:

$$\varepsilon_{c,dc} = 0.004 + 1.4\frac{\rho_v f_{yh}\varepsilon_{su}}{f'_{cc}} \quad (45)$$

where ε_{su} is a strain value at fracture of lateral confining ties, and ρ_v is the volumetric confinement ratio, which is the sum of ρ_x and ρ_y.

3.3.3 Geometric Nonlinearity

Large displacements, large rotations, and large independent deformations relative to the chord of the frame element cause nonlinearities in kinematic quantities, these sources of nonlinearity are referred to as geometric nonlinearities, also known as p-delta effects. These nonlinearities are negligible under normal load conditions but they become significant in the presence of extreme loads and large/slender structures. The internal forces demand is amplified under large lateral deflections, which results in a reduction in the effective lateral stiffness. The potential capacity of the structure to resist lateral loads decreases as internal forces rise, resulting in a drop in the structure's effective lateral strength. Since they may eventually result in the loss of lateral resistance, ratcheting, and dynamic instability, this warrants consideration in the numerical models (Deierlein *et al*., 2010).

A total co-rotational formulation developed by Correia and Virtuoso (2006) is used to take into account the large displacements/rotations and large independent deformations relative to the chord of the frame elements in the model. The total co-rotational formulation makes use of an exact description of the kinematic transformations associated with large displacements and three-dimensional rotations of the element. As a result, the independent deformations and forces of the element are correctly defined, and the effects of geometric non-linearities on the stiffness matrix are naturally defined. The use of this formulation takes into account small deformations in relation to the element's chord without losing its generality, despite the existence of large nodal rotations and displacements.

3.4 Modeling of Fixed-End Rotation

The fixed-end rotation at the interface of the beam and column caused by bond failure, longitudinal rebar-slip, and inelastic extension is simulated for each element using a single nonlinear rotational spring located at the beam-column member ends (Figure 11a) and a concentrated plasticity hinge with a nonlinear moment-rotational behavior (Figure 11b, Table 1) is used to model the rigid-body rotational deformation of the member. The formulation developed herein for fixed-end rotation is similar to the rigid-bar rotation model proposed by Filippou and Issa (1988) with the improvement including a more realistic representation of the moment-rotation relationship developed recently by Ahmad *et al.* (2020) based on quasi-static cyclic tests performed on full-scale beams exhibiting fixed-end rotation. A trilinear force-deformation envelope is proposed to model inelastic mechanisms (cracking, yielding, and rocking) with a deteriorating hysteretic rule to model stiffness and strength deterioration and pinching behavior. Due to its high initial stiffness, the hinge may only contribute marginally before the beam yields but contributes significantly after the rocking mode is initiated.

Preprints (www.preprints.org) | NOT PEER-REVIEWED | Posted: 4 October 2022 doi:10.20944/preprints202210.0017.v1

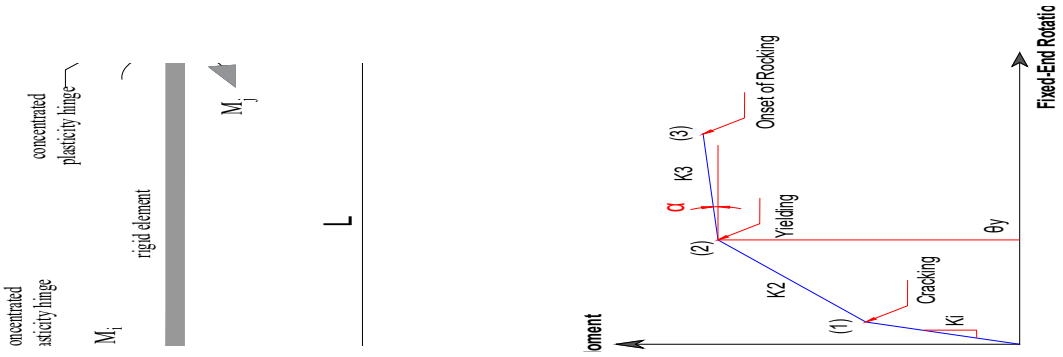

(a) Beam-column element with ends plasticity hinge

(b) Moment-rotational relationship (Ahmad *et al*., 2020)

Figure 11. Analytical model for a beam-column element with fixed-end rotation: (a) concentrated plasticity hinges at beam ends and (b) proposed moment-rotation relationship based on experimental studies performed on full-scale beams.

Table 1. Proposed moment-rotation values for fixed-end rotational spring to model beam-column member rigid-body rotational deformation (Ahmad *et al*., 2020)

Parameter	θ_{cr} (rad)	M_{cr}/M_{max}^*	θ_y (rad)	M_y/M_{max}^*	$\alpha = K_3/K_1$
Value	0.00091	0.27	0.01177	0.76	0.055

*M_{max} *is the beam maximum moment capacity.*

The flexibility matrix's off-diagonal components may simply be demonstrated to be zero in this situation and as a result, the flexibility matrix of the element is given:

$$F_{FER} = \begin{bmatrix} f_i & 0 \\ 0 & f_j \end{bmatrix} \tag{46}$$

where f_i is the flexibility coefficient of the rotational spring at the end i and f_j is the flexibility coefficient of the rotational spring at end j. Assuming that the point of inflection remains fixed and lies in the middle of the beam throughout the loading history, in this case, each half of the member can be viewed as a cantilever beam and the flexibility coefficients can be easily formulated. The problem can be further simplified, ignoring gravity load, this corresponds to a cantilever beam subjected to load P (Figure 12).

To determine the flexibility coefficients of the concentrated hinge, the rotation at the cantilever's root (beam ends) caused by the curvature distribution is first determined for various values of the load P, and if the moment-curvature relation is known, this can be simplified. The moment-rotation relationship proposed (Figure 11b) is trilinear, due to which the approach produces a nonlinear flexibility coefficient of the corresponding concentrated spring. The stiffness of the hinge can be determined as:

$$K_i = \frac{M_{cr}}{\theta_{cr}} \qquad 0 \le M \le M_{cr} \tag{47}$$

$$K_2 = \frac{M_y - M_{cr}}{\theta_y - \theta_{cr}} \qquad M_{cr} \le M \le M_y \tag{48}$$

$$K_3 = \frac{M - M_y}{\theta - \theta_y} \qquad M_y \le M \tag{49}$$

where K_i is the initial stiffness, K_2 is the post-cracking stiffness, and K_3 is the post-yield stiffness of the hinge. The limit state values of moment (M) and rotation (θ) are given in Table 1.

Preprints (www.preprints.org) | NOT PEER-REVIEWED | Posted: 4 October 2022 doi:10.20944/preprints202210.0017.v1

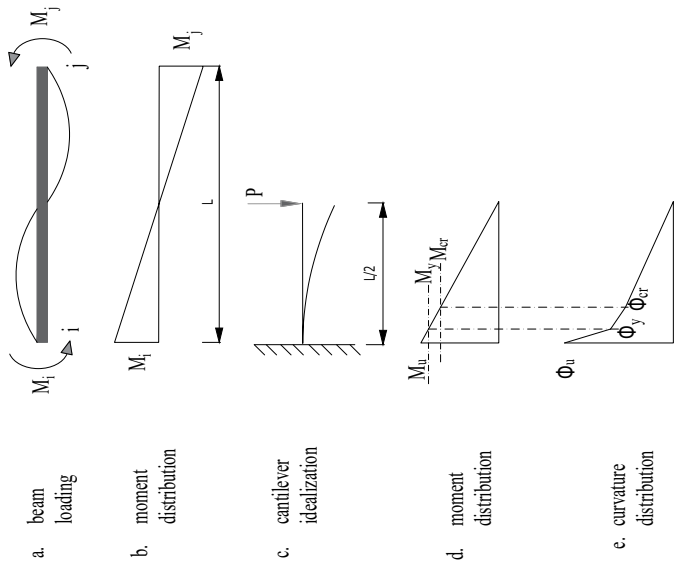

Figure 12. Mechanical parameters of fixed-end rotation beam-column member. Considering only the rigid-body rotation mode of the beam.

It is typical to represent the flexibility matrix of a rotational spring stiffness *K* in terms of the prismatic beam element's elastic stiffness for convenience:

$$K_i = \frac{4.EI}{\gamma.L} \tag{50}$$

$$K_2 = \beta_1 \frac{4.EI}{\gamma.L} \tag{51}$$

$$K_3 = \beta_2 \frac{4.EI}{\gamma.L} \tag{52}$$

where γ, β_1, and β_2 are coefficient vary as a function of the moment-rotation demand. The experimental data suggests $\beta_1 = 0.165$ and $\beta_2 = 0.055$, and $\gamma = 0.406$ if *EI* is based on the nominal moment and yield curvature of the beam section (Ahmad *et al.*, 2020). The flexibility matrix can be formulated as given:

$$F_{FER,1} = \frac{L}{6EI}\begin{bmatrix} 1.5\gamma_i & 0 \\ 0 & 1.5\gamma_j \end{bmatrix} \qquad 0 \le M \le M_{cr} \tag{53}$$

$$F_{FER,2} = \frac{L}{6EI.\beta_1}\begin{bmatrix} 1.5\gamma_i & 0 \\ 0 & 1.5\gamma_j \end{bmatrix} \qquad M_{cr} \le M \le M_y \tag{54}$$

$$F_{FER,3} = \frac{L}{6EI.\beta_2}\begin{bmatrix} 1.5\gamma_i & 0 \\ 0 & 1.5\gamma_j \end{bmatrix} \qquad M_y \le M \tag{55}$$

This concentrated plasticity model has the advantage of being computationally simple can be readily implemented in a finite element computer program and can accurately represent the hysteretic response of RC members whose behavior is controlled by fixed-end rotation. The flexibility matrix of the element is calculated by simply adding the flexibility matrices of the constituent elements (i.e. beam-column inelastic member and concentrated plasticity hinge), since the plasticity hinge element and the inelastic beam-column member act in series.

4. Validation of the Proposed Modeling Technique

4.1. Quasi-Static Cyclic Testing of Tee Beam-Column Joint

4.1.1 Description of Test Specimen

Preprints (www.preprints.org) | NOT PEER-REVIEWED | Posted: 4 October 2022 doi:10.20944/preprints202210.0017.v1

A low-rise building was considered as a prototype for choosing the geometric and reinforcement detailing of a typical substandard beam-column joint (Badrashi, 2016) in order to study the behavior of deteriorating joints and serve as a benchmark for testing and validating the proposed numerical modeling technique. Several deficiencies were discovered during the field survey of reinforced concrete building stock in Pakistan (Badrashi, 2016). Because it was not possible to include all of the defects in the experimental models due to time and financial constraints, it was chosen to analyze just those deficiencies that would have a significant influence on the seismic performance of the reinforced concrete buildings in Pakistan.

The selected beam-column joint subassembly (Figure 13) included columns that were 12 inches wide and 12 inches deep, and a beam that was 12 inches wide and 18 inches deep. This model took into account all deficiencies found between design standards and actual reinforced concrete building constructions in Pakistan. These deficiencies included: spacing of ties - double of specified spacing, lack of seismic hooks, location of splice-near beam-column joint, lap length-reduced by 45%, 20% reduction in dia of rebars, lack of ties in beam-column joint core (except a single tie), concrete having compressive strength of 2000 psi, and rebars had yield strength of 40,000 psi. The model's beam is reinforced with 3#5 bars at the top and bottom to represent the use of undersized reinforcing bars in constructions. A #3 stirrup was used as the lateral tie in the beam, positioned uniformly at 6 inch on centers. There are no seismic hooks and the ties are closed at a 90-degree angle.

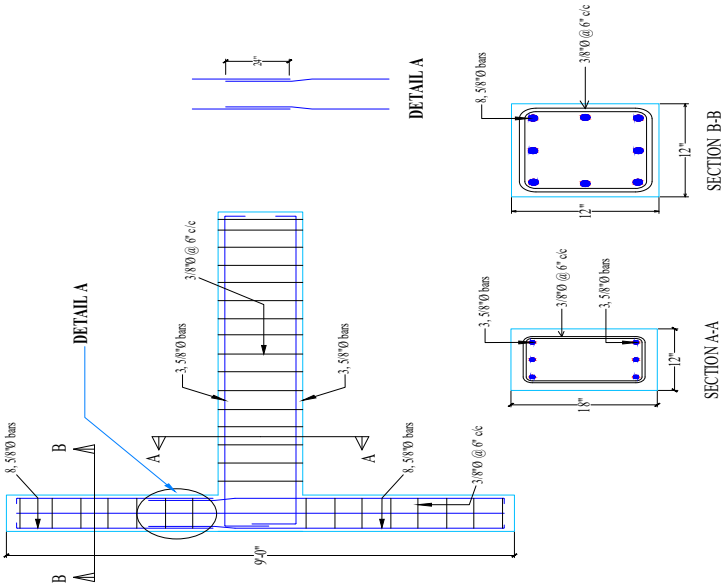

Figure 13. Geometric and reinforcement details of substandard beam-column joint

4.1.2 Experimental Program and Specimen Behavior

Figure 14 illustrates the selected test setup and loading of the beam-column joint. The load is applied directly at the point of contra flexure of the beam (i.e. free end of T-joint). Boundary conditions were selected to accurately reflect the end restraints of a two-dimensional frame. A hinge support was used to pin-connect the bottom of the column: pins were firmly fastened to a steel girder, and that steel girder was in turn fastened to the strong floor. The top of the column was provisioned with a roller support to enable unrestricted movement in vertical direction while the lateral movement was restricted.

Preprints (www.preprints.org) | NOT PEER-REVIEWED | Posted: 4 October 2022 doi:10.20944/preprints202210.0017.v1

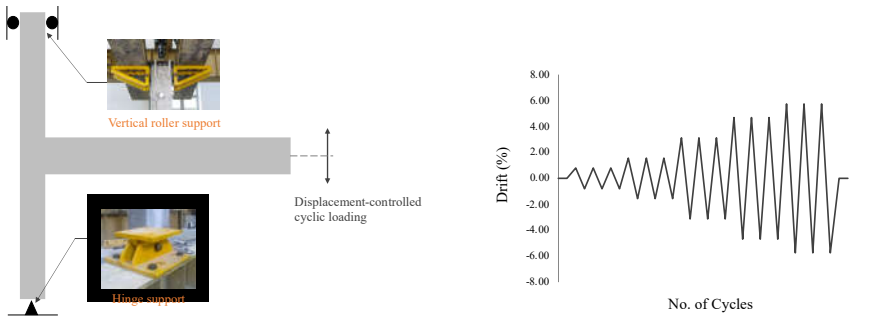

(a) Test Setup (b) Cyclic Displacement Loading

Figure 14. Schematic representation of test specimen setup and loading

A permanent gravity load of 26 tons (20% of the gross-section capacity) was applied at the top of the column. A reverse cyclic load was applied at the beam end of the beam-column assembly. To simulate the pre-cracked conditions, initially the assembly was tested under force-controlled loading. First, three tons of load was determined to be the theoretical yield capacity F_y of the system. This was used to guide load control testing, the force was applied in four equal increments: $0.25F_y$, $0.5\ F_y$, $0.75F_y$ and F_y, and each increment was repeated three times. This was followed by displacement-controlled testing till the specimen attained extensive damages (Figure 16). Initially, the assembly was tested under force-controlled loading to simulate the pre-cracked conditions of existing buildings. The system's theoretical yield capacity, F_y, was first determined to be **03** tons. The force was applied in four equal increments—0.25Fy, 0.5Fy, 0.75Fy, and Fy—and each increment was repeated three times during the load control tests. Displacement controlled testing was conducted after that until the specimen had sustained extensive damages (Figure 15).

Diagonal cracks initiated in the beam-column joint and vertical cracks appeared at the beam-column interface at a drift demand of 1.0%. The existing cracks in joints aggravated and additional multiple cracks were appeared with increasing drift demand from 1.5% to 3.0% drift. Consequently, concrete wedge mechanism was initiated. Upon further increasing drift demand the width of existing cracks widened while concrete wedge was detached from the joint at a drift demand of 5.0%. This failure mechanism is especially brittle, and the bearing load capacity is lost as a result of the pushing out of a concrete wedge, therefore, the test was terminated.

4.2. Comparison of Numerical to Experimental Prediction

The analytical model illustrated in Figure 5 is generated using the nonlinear finite element SeismoStruct program. The analytical model constitutes the inelastic beam and column members modeled as inelastic fibre section-based elements that use the force-based formulation with the improved materials models discussed earlier. The material model for rebars is a uniaxial steel model that was first developed by Monti *et al.* (1996) and can comprehend the post-elastic buckling behavior of reinforcing bars in compression. It makes use of the stress-strain relationship presented by Menegotto and Pinto (1973) as well as the isotropic hardening rules of Filippou *et al.* (1983) and the buckling rules of Monti and Nuti (1992). For increased numerical stability/accuracy under transient seismic stress, it considers a further memory rule suggested by Fragiadakis *et al.* (2007). The material model for concrete is a uniaxial nonlinear constant confinement model described earlier that was first developed by Madas (1993) and adheres to the stress-strain relationship established by Mander *et al.* (1988) and the cyclic rules proposed by Martinez-Rueda and Elnashai (1997). The Mander *et al.* (1988) rule, which assumes continuous confining pressure over the whole stress-strain range, integrates the confinement effects offered by the lateral transverse reinforcement.

Preprints (www.preprints.org) | NOT PEER-REVIEWED | Posted: 4 October 2022 doi:10.20944/preprints202210.0017.v1

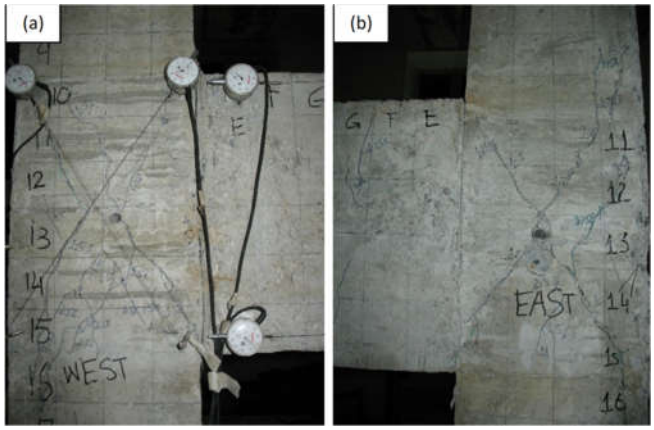

(Damages at 3.0% Drift)

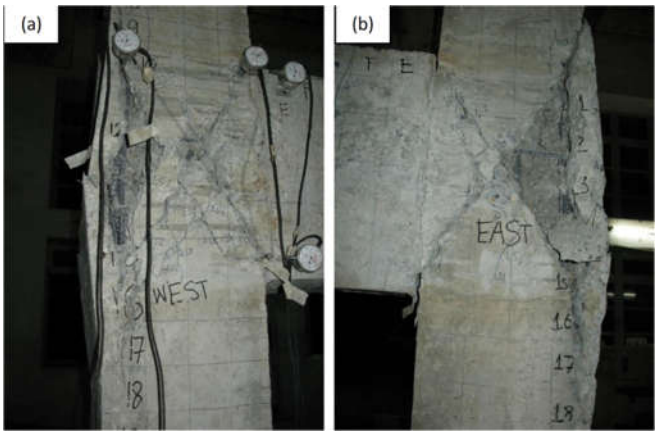

(Damages at 5.0% Drift)

Figure 15. Damages observed in beam-column joint with increasing drift demand. (a) represents west side face and (b) represents east side face.

To simulate the fixed-end rotation, a concentrated plasticity hinge is introduced at the beam end using zero-length link element. The link element connects two contemporaneous structural nodes and necessitates the development of a separate force-displacement (or moment-rotation) response curve for each of its local six degrees of freedom. An infinitely stiff elastic force-displacement rule is assigned to all degrees of freedom, except the in-plane rotational dof that was assigned with the multilinear moment-rotation rule (Figure 11b) featuring pinching in the hysteretic force-displacement behavior to simulate the opening/closing of vertical crack at the beam end. The selected hysteresis loop is described in Sivaselvan and Reinhorn (1999), which is capable of simulating the deterioration of strength, stiffness, and bond slip. The vertical dof of link element was assigned with linear force-displacement behavior to idealize the beam elastic shear deformation.

Four stiff link elements are positioned along the edges of the panel to idealize the joint panel, and one nonlinear moment-rotation spring was introduced at one corner hinge. The backbone moment-rotation curve represents the behavior for monotonic loading and establishes strength and deformation bounds (Figure 6a), and uses a pinched hysteretic model of Ibarra *et al.* (2005) to model deteriorating hysteresis of the backbone curve (Figure 6b).

Figure 16 compares the analytical and experimental hysteretic responses of the Tee beam-column joint. This demonstrates that the initial stiffness, maximum strength, and hysteretic response of the analytical model agree well with the experimental response. The proposed joint modeling technique accurately simulates the inelastic response of the Tee beam-column joint viz. the plastic hinge flexural damage mechanism with slip of the

Preprints (www.preprints.org) | NOT PEER-REVIEWED | Posted: 4 October 2022 doi:10.20944/preprints202210.0017.v1

reinforcing bars in the inelastic beam member and joint damage shear hinge mechanism within the panel zone, as well as the deterioration of stiffness and strength important for the considered substandard beam-column joint. Therefore, the proposed joint panel idealization using a nonlinear zero-length rotational spring with a deteriorating hysteretic rule may accurately model the nonlinear behavior of the exterior beam-column joints in existing structures.

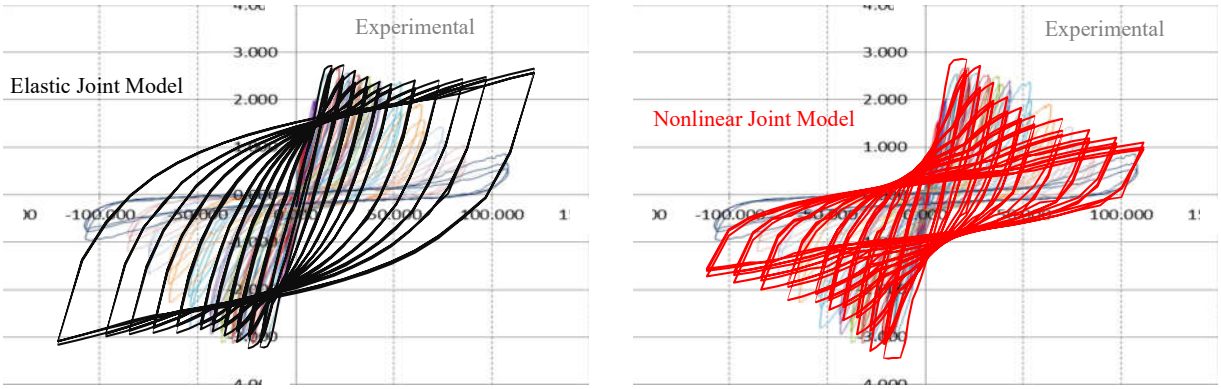

(a) (b)

Figure 16. Comparison of the analytical to experimental force-displacement hysteretic responses. Model with elastic joints and conventional beam-column element formulation is shown in (a) and proposed model with nonlinear joints and improved beam-column element formulation is shown in (b). displacement is given in mm and force is given in ton.

5. Frame Structure Nonlinear Response Analysis

5.1. Description of Frame Structure

A five-story reinforced concrete moment-resisting frame structure in the present study serves as a representative example of a Pakistani substandard frame building construction that falls short of code requirements (Figure 17). The assumed footprint of the structure is 45.72 m (150 ft) by 36.576 m. (120 ft). The structure has five bays in each direction, with the following dimensions: 9.144 m (30 ft) longitudinal bay width, 7.3152 m (24 ft) transverse bay width, and 3.6576 m story height (12 ft).

In compliance with the building regulation, a live load of 2.40 kN/m^2 was taken. A 203 mm (8 in) thick two-way floor slab and a superimposed dead load of 1.0 kN/m^2 (20 lbs/ft^2) were included in the dead load in addition to the members' self-weight. The beams and columns were designed using regular reinforced concrete with a 28-day unconfined compressive strength of 13.80 MPa (2000 psi). The weight of the concrete is taken 23.60 kN/m^3 (150 lbs/ft^3). Reinforcement steel of grade 40 with a design yield tensile strength of 276 MPa (40 ksi) was used. Building analysis and design were performed for the short direction in accordance with the BCP-SP (2007), assuming a fixed base to signify an adequate foundation.

A single-bay, two-dimensional, multi-story frame was extracted for nonlinear modeling and building response analysis. Based on the tributary area, weights were applied to the single-bay frame. Due to the same structural and dynamic properties that follow (i.e. building vibration period, frame damage mechanisms, and nonlinearities), it is intended that the behavior of the buildings resemble that of a planar frame. While other 3-dimensional effects and the slab contribution can affect a structure's seismic response (Masoudi and Khajevand, 2020), the planar frame simplification allows for a significant reduction in the number of elements and degrees of freedom in the numerical model, which reduces the computation time needed for the building nonlinear response analysis and is a conservative approach to assessment.

Preprints (www.preprints.org) | NOT PEER-REVIEWED | Posted: 4 October 2022 doi:10.20944/preprints202210.0017.v1

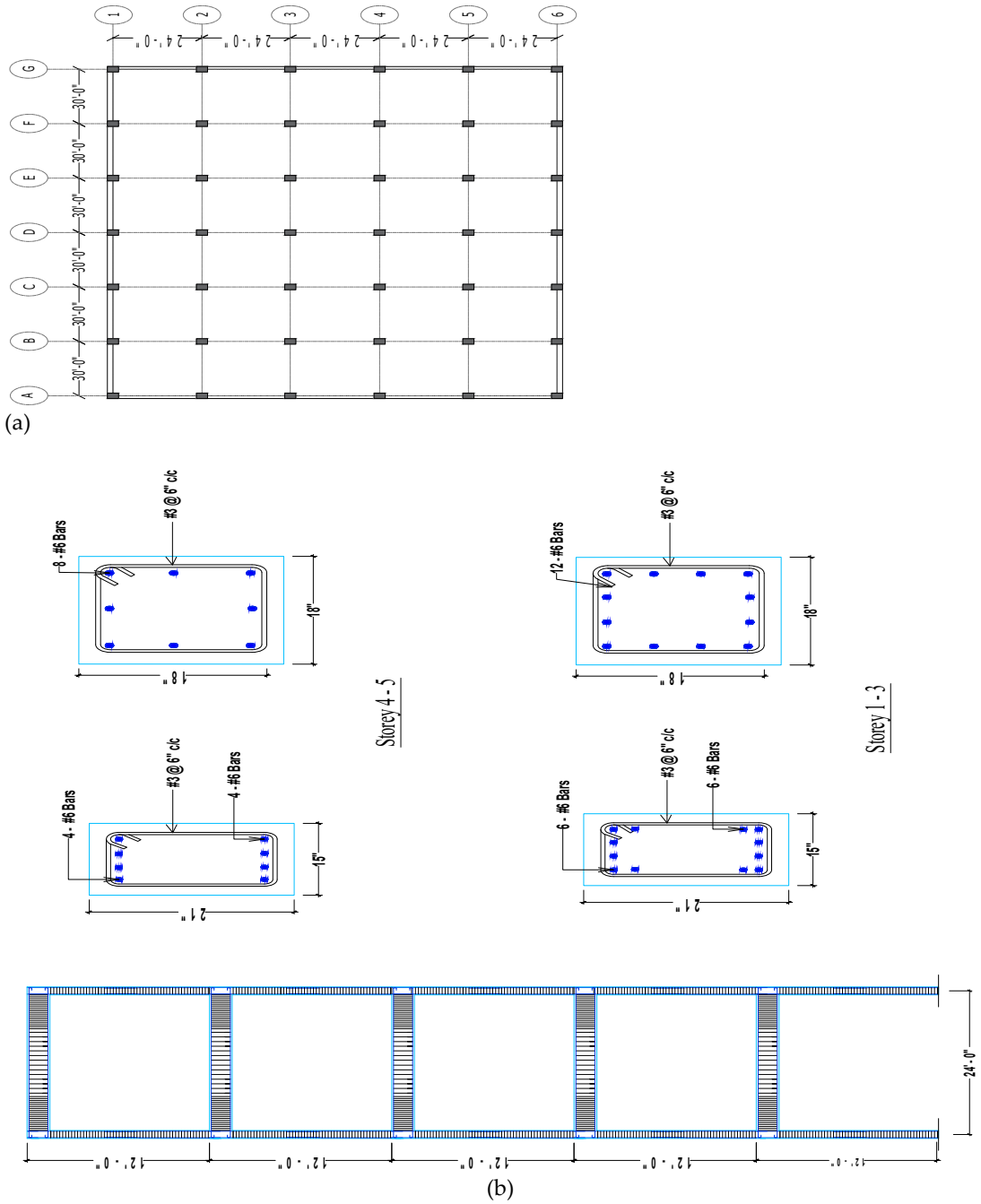

Figure 17. Geometric and reinforcement details of the selected frame. (a) The footprint of the considered building and (b) one-bay multi-story frame extracted for nonlinear response analysis.

5.2. Numerical Modeling

The nonlinear finite element SeismoStruct program was used to numerically model the considered prototype multi-story frame in a manner similar to the Tee beam-column joint discussed earlier. The floor loads and masses are lumped evenly at floor structural nodes. In order to account for the large displacements, the total corotational geometric transformation was used (Correia and Virtuoso, 2006). According to earlier research, the mass and stiffness proportional Rayleigh damping in the first two modes was set at 2% of critical for the considered frame (Ahmad *et al.*, 2020). The building frame elements were discretized using the fibre section-based element with mixed formulation developed by Spacone *et al.* (1996a, 1996b) that uses the improved material model formulations

Preprints (www.preprints.org) | NOT PEER-REVIEWED | Posted: 4 October 2022 doi:10.20944/preprints202210.0017.v1

(Fragiadakis *et al*., 2007; Martinez-Rueda and Elnashai, 1997). To account for the fixed-end rotation caused by bond failure, rebars yielding, and inelastic extension, the frame elements were provided with concentrated plasticity hinges that maintain the formulation of Filippou *et al*. (1983) and uses the pinched degrading hysteretic rule as proposed by Sivaselvan and Reinhorn (1999). The frame was idealized using elastic joints (center-line model), and nonlinear joint panel models with deterioration of stiffness and strength to evaluate the significance of the improved formulation. The joint panels are idealized as a parallelogram of stiff elements and provisioned with a corner nonlinear moment-rotation spring that uses the pinched deteriorating hysteresis of Ibarra *et al.* (2005).

5.3. Selected Ground Motions

Twenty-four far-fault earthquake ground motions were obtained from the PEER NGA online ground motion database. Given that an existing structure may experience a variety of moderate-to-strong ground motions throughout its design life, it was preferable to subject the numerical model to a range of ground motions that represented variation in the key seismological parameters, such as magnitude (Mw: 6 to 7.62), fault mechanism (reverse, reverse-oblique, and strike-slip), source-to-site distance (Rjb: 17 km to 29 km), and significant duration (D5-95%: 11 sec to 70. A single ground motion from each earthquake event was chosen in order to account for record-to-record variability. Earthquake events from numerous active tectonic zones (US, Japan, New Zealand, Iran, Taiwan, Armenia, Mexico) were taken into consideration. The median spectrum for the elastic 5% damped single degrees of freedom systems with periods ranging from 0.02 sec to 4.0 sec and subjected to unscaled ground movements is shown in Figure 18, and reported in Table 2. The selected unscaled ground motions have a peak acceleration of 0.35g at a period of 0.26 sec and a median peak ground acceleration of 0.16g.

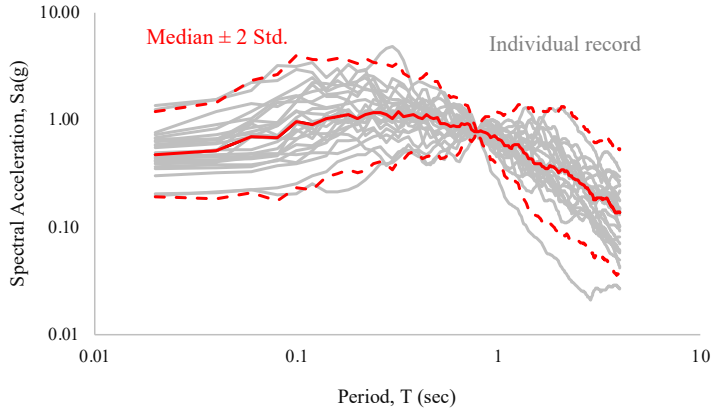

Figure 18. Acceleration response spectrum of the selected twenty-four ground motions linearly scaled and conditioned on the building period T_1 = 0.78 sec.

5.4. Frame Nonlinear Response

5.4.1. Damage Distribution

The seismic response of the selected frame is evaluated using a nonlinear response history analysis procedure, with both a conventional frame model with elastic joints and an improved frame model with nonlinear joint model and improved element formulation taken into account.

Table 2. Details of the ground motions used for nonlinear response history analysis. Rev. represents reverse fault, Rev. Ob. represents reverse and oblique fault, and SS represents strike-slip fault.

S. No.	Earthquake Event	Year	Recording Station	Mw	Fault	Rjb (km)	Duration (sec), 5-95%

Preprints (www.preprints.org) | NOT PEER-REVIEWED | Posted: 4 October 2022 doi:10.20944/preprints202210.0017.v1

1	San Fernando	1971	LA - Hollywood Stor FF	6.61	Rev.	22.77	13.4
2	Tabas_ Iran	1978	Boshrooyeh	7.35	Rev.	24.07	19.5
3	Coalinga-01	1983	Parkfield - Fault Zone 15	6.36	Rev.	28.00	19.7
4	Spitak_ Armenia	1988	Gukasian	6.77	Rev. Ob.	23.99	10.5
5	Loma Prieta	1989	Hollister - South & Pine	6.93	Rev. Ob	27.67	28.8
6	Northridge-01	1994	LA - W 15th St	6.69	Rev.	25.59	20.2
7	Chi-Chi_ Taiwan	1999	CHY025	7.62	Rev. Ob.	19.07	35.3
8	St Elias_ Alaska	1979	Icy Bay	7.54	Rev.	26.46	34.6
9	Niigata_ Japan	2004	NIG018	6.63	Rev.	21.55	70.3
10	Chuetsu-oki_ Japan	2007	Joetsu Kita	6.80	Rev.	28.97	30.8
11	Iwate_ Japan	2008	IWT012	6.90	Rev.	20.47	30.8
12	Christchurch_ New Zealand	2011	LINC	6.20	Rev. Ob.	18.47	13.3
13	Northern Calif-03	1954	Ferndale City Hall	6.50	SS	26.72	19.4
14	Imperial Valley-06	1979	Delta	6.53	SS	22.03	51.4
15	Victoria_ Mexico	1980	Chihuahua	6.33	SS	18.53	19
16	Morgan Hill	1984	Agnews State Hospital	6.19	SS	24.48	40.9
17	Superstition Hills-02	1987	Brawley Airport	6.54	SS	17.03	14.3
18	Landers	1992	North Palm Springs	7.28	SS	26.84	37.9
19	Kobe_ Japan	1995	Fukushima	6.90	SS	17.85	35.7
20	Tottori_ Japan	2000	OKY005	6.61	SS	28.81	24
21	Parkfield-02_ CA	2004	Coalinga - Fire Station 39	6.00	SS	22.45	27.7
22	El Mayor-Cucapah_ Mexico	2010	Chihuahua	7.20	SS	18.21	51.2
23	Joshua Tree_ CA	1992	Thousand Palms Post Office	6.10	SS	17.15	11.1
24	Darfield_ New Zealand	2010	WSFC	7.00	SS	24.36	26.2

The ground motion of Kocaeli Turkey earthquake of August 17, 1999 (recording station: YARIMC, KOERI330; Source: PEER Strong Motion Database) was considered and scaled linearly by a factor of 1.75 to induce large nonlinearity in the frame for contrasting the behavior of frames. Member chord rotation indicates the extent of plasticity the member experience during ground motion, which is an important indicator of seismic damage distribution. Damage distribution diagrams are developed (Figure 18), depicting elements' maximum chord rotation values (in percentage) to graphically compare the effects of joint modeling on the damage distribution. Shear hinge formation in the joints is also reported. The joint damage corresponds to the initiation of diagonal cracking when the principal tensile stress in the joint exceeds $0.29(f_c')^{0.5}\ MPa$; moderate damage when the principal tensile stress in the joint is between $0.29(f_c')^{0.5}\ MPa$ and $0.42(f_c')^{0.5}\ MPa$; and extensive damages in the panel zone when the principal tensile stress in the joint exceeds $0.42(f_c')^{0.5}\ MPa$. Due to the flexibility that joint deformation provides, the activation of the joint shear mechanism increases the chord rotation demand on the connecting beam members. The performance of the conventional frame with elastic joints is satisfactory under the considered ground motions. The improved model, on the other hand, shows critical shear mechanism and increased member chord rotation demand sufficient to cause soft-story mechanism and consequent frame collapse.

Preprints (www.preprints.org) | NOT PEER-REVIEWED | Posted: 4 October 2022 doi:10.20944/preprints202210.0017.v1

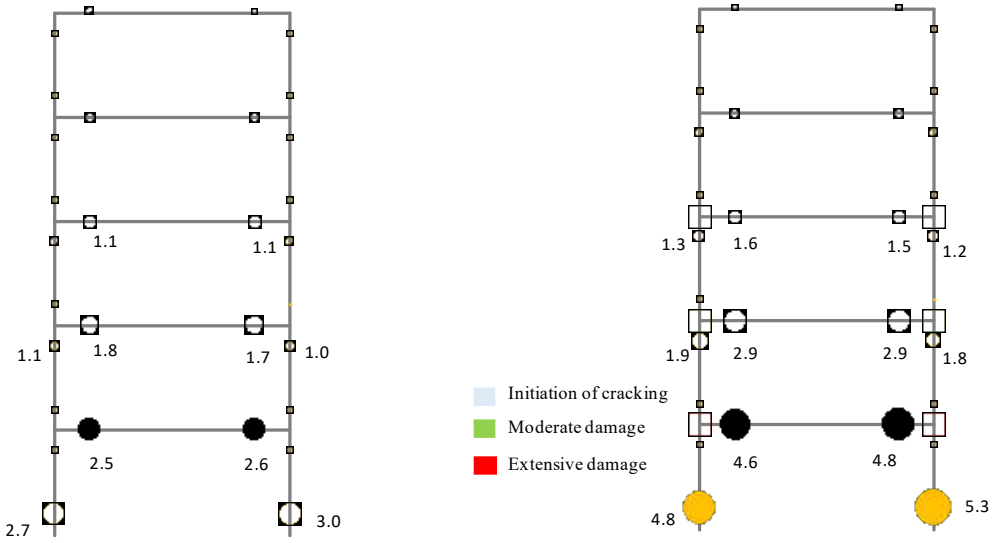

(a) Conventional model (b) Improved model

Figure 18. Response comparison for a five-story frame using a conventional model with elastic joint (a) and model with nonlinear joint model and improved frame element formulation. The member chord rotation value is given in percentage.

5.4.2. Inter-Story Drift Demand

The maximum inter-story drift ratio per record is obtained in order to evaluate the modeling technique with regard to the distribution of lateral deformation demand. Figure 19 shows the distribution of the maximum inter-story drift values while taking the average of the suite of ground motions. The inter-story drift distribution emphasizes the significance of the joint nonlinear model and the improved element formulation because, when compared to the drift demand for a conventional frame model, the drift demand for the frame model increases when joint nonlinearity is included and the improved element formulation is used. For the improved frame model with nonlinear joints, an increase of up to 62% (mean drift) and 89% (mean+1.std.) is shown in the lower floors when assessing the inter-story drift distribution. As a result, the frame drift responses are drastically underestimated by the conventional frame model.

5.4.3. Collapse Risk

According to the experimental results discussed earlier, 4.50% of story drift is a realistic approximation for the beam-column connection's collapse limit since, after this drift limit was exceeded, the joint lost its ability to support the gravity loads. Figure 20 reports the maximum story drift demand for each individual ground motion. Comparing the maximum story drift demand for different ground motions can give the instances the demand exceeds the capacity. We observed 7 instances of the demand exceeding the capacity in the case of an improved frame model, resulting in a collapse risk of 7/24 = 0.292 (probability of failure = 29.20%). However, in the case of the conventional frame model, there is only one event where the demand exceeds the capacity, which results in a collapse risk of 1/24 = 0.042 (probability of failure = 4.20%). The relevant fitting procedure for fitting fragility functions that use the maximum likelihood method, as outlined by Baker (2015), was used to derive fragility functions for the considered frames. Figure 21 shows the fragility functions of both conventional and improved frame models, indicating the conventional model grossly underestimates the collapse risk of frames.

Preprints (www.preprints.org) | NOT PEER-REVIEWED | Posted: 4 October 2022 doi:10.20944/preprints202210.0017.v1

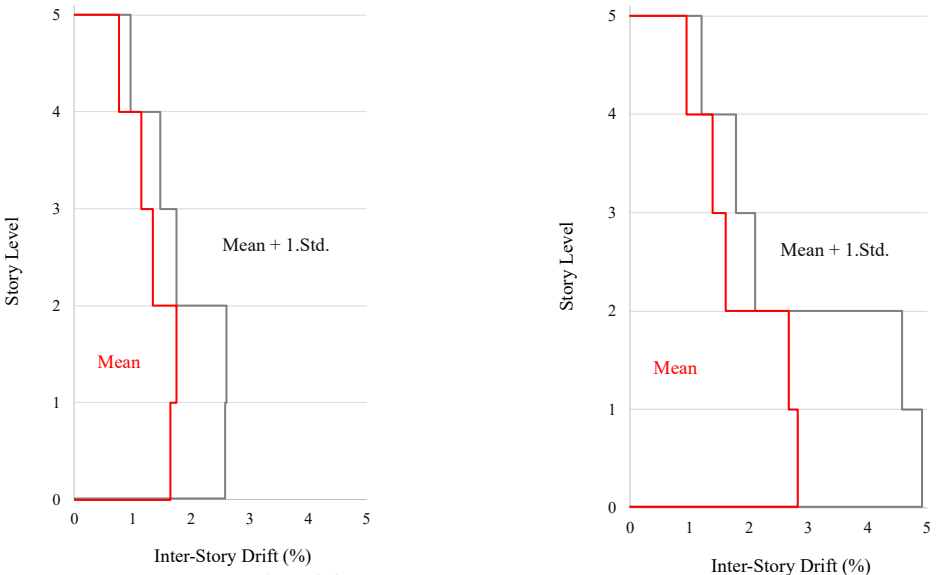

Figure 19. Inter-story drift comparison for a five-story frame using a conventional model with elastic joint and model with nonlinear joint model and improved frame element formulation.

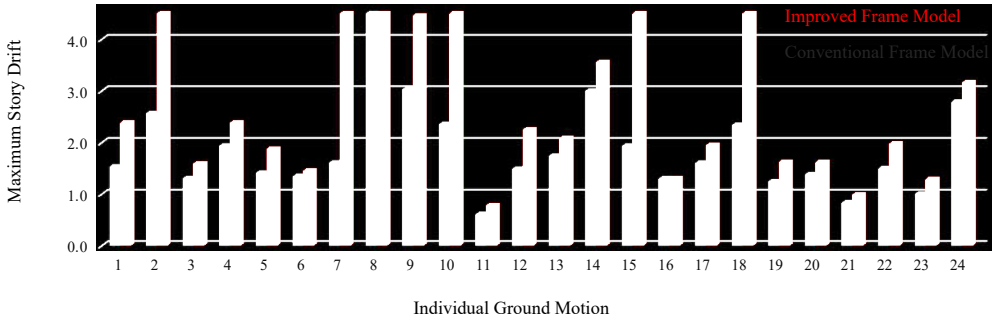

Figure 20. The maximum story drifts demand in individual ground motion for both conventional and improved frame models.

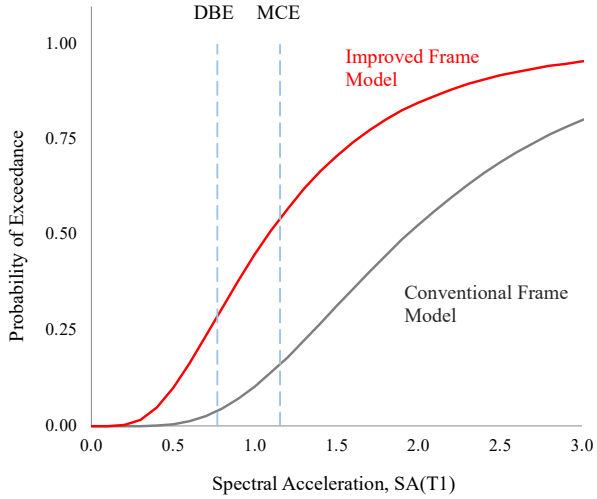

Figure 21. Collapse fragility functions for conventional and improved frame models.

 doi:10.20944/preprints202210.0017.v1

6. Conclusions

The majority of existing nonlinear modeling techniques are deficient in one or more crucial characteristics, making them less appropriate for simulating the nonlinear behavior of substandard beam-column joints that exhibit deterioration of stiffness and strength. In order to effectively model and simulate the deteriorating response of substandard beam-column joints, as demonstrated in the experimental test and supported by numerical simulation, fixed-end rotation must be taken into consideration in addition to joint nonlinearity. To accurately determine the member stiffness matrix, resisting forces, and deformation, it is therefore necessary to improve the conventional nonlinear finite element fibre-section based element to account for the appropriate section/element force-deformation behavior. The importance of accurate nonlinear modeling becomes evident when assessing the performance of structures for strong ground motions, as the collapse risk is grossly underestimated when using conventional modeling techniques in contrast to a more accurate nonlinear model. It is of particular importance when determining the collapse risk of structures for strong ground shaking with a large duration, and it becomes crucial in the case of reverse/oblique faults because most collapses are observed in earthquakes caused by these faults.

Supplementary Materials: Requests for the data presented here can be sent to drnaveed@stanford.edu

Author Contributions: Conceptualization, N.A., M.R.; methodology, N.A., M.R., B.I., S.H.; software, N.A., M.R., B.I., M.E.A., S.H., H.S.; validation, N.A., M.R.; formal analysis, N.A., M.R., M.E.A.; investigation, N.A., M.R., M.E.A., S.H.; resources, N.A., M.R., M.E.A., S.H., M.U.K, H.S.; data curation, N.A., M.E.A.; writing—original draft preparation, N.A., M.E.A.; writing—review and editing, M.R., B.I., S.H., M.U.K., H.S.; visualization, N.A., M.E.A., S.H.; supervision, N.A.; project administration, N.A., M.E.A. All authors have read and agreed to the published version of the manuscript.

Funding: This research received no external funding.

Data Availability Statement: Requests for the data presented here can be sent to drnaveed@stanford.edu.

Acknowledgments: The first author is grateful to the United States Educational Foundation in Islamabad for sponsoring his Visiting Scholar appointment at Stanford University under the Fulbright Scholar program.

Conflicts of Interest: The authors declare no conflict of interest.

References

1. ACI-352-R02. 2002. Recommendations for the design of beam-column joints in monolithic reinforced concrete structures. American Concrete Institute (ACI), Farmington Hills, Michigan, USA.
2. Ahmad N., Rizwan M., Ashraf M., Khan A.N. and Ali Q. 2020. Seismic collapse safety of reinforced concrete moment resisting frames with/without beam-column joint detailing. *Bulletin of the New Zealand Society for Earthquake Engineering* 54(1), 1-20.
3. Ahmad N., Shahzad A., Rizwan M., Khan A.N., Ali S.M., Ashraf M., Naseer A., Ali Q. and Alam B. 2019. Seismic performance assessment of non-compliant SMRF reinforced concrete frame: shake-table test study. *Journal of Earthquake Engineering*, 23(3), 444-462.
4. Alath S. and Kunnath S.K. 1995. Modeling inelastic shear deformations in RC beam-column joints. *Proceedings of 10th Engineering Mechanics Conference*, ASCE, 822-825.
5. Alemdar B.N. and White D.W. 2005. Displacement, flexibility, and mixed beam-column finite element formulations for distributed plasticity analysis. *Journal of Structural Engineering* 131(12), 1811-1819.
6. Altoontash, A. 2004. Simulation and damage models for performance assessment of reinforced concrete beam-column joints. *PhD Dissertation*, Department of Civil and Environmental Engineering, Stanford University, CA, USA.
7. Aycardi L.E., Mander J.B. and Reinhorn A.M. 1994. Seismic resistance of reinforced concrete frame structures designed only for gravity loads – experimental performance of subassemblages. ACI Structural Journal, 91(5), 552–63.
8. Baber T.T. and Noori M.N. 1985. Random vibration of degrading pinching systems. *Journal of Engineering Mechanics ASCE* 111(8), 1010-1026.
9. Baker J.W. 2015. Efficient analytical fragility function fitting using dynamic structural analysis. *Earthquake Spectra* 31(1): 579-599.
10. BCP-SP. 2007. *BCP-SP: Building Code of Pakistan – Seismic Provisions*. Ministry of Housing and Works, Islamabad.
11. Beres A, Pessiki S.P., White R.N., Gergely P. 1996. Implications of experiments on the seismic behaviour of gravity load designed RC beam-to-column connections. *Earthquake Spectra* 12(2), 185-98.

12. Biddah A. and Ghobarah A. 1999. Modelling of shear deformation and bond slip in reinforced concrete joints. *Structural Engineering and Mechanics* 7(4), 413-32.
13. Calabrese A., Almeida J.P., Pinho R. 2010. Numerical issues in distributed inelasticity modelling of RC frame elements for seismic analysis. *Journal of Earthquake Engineering*, 14(S1), 38-68.
14. Calvi G.M., Magenes G. and Pampanin S. 2002. Relevance of beam-column joint damage and collapse in RC frame assessment. *Journal of Earthquake Engineering* 6(1), 75-100.
15. Ciampi V. and Carlesimo L. 1986. A nonlinear beam element for seismic analysis of structures. *Proceedings of the 8th European Conference on Earthquake Engineering*, Lisbon, Portugal.
16. Correia A.A. and Virtuoso F.B.E. 2006. Nonlinear analysis of space frames. In: Mota Soares et al. III European Conference on Computational Mechanics. Springer, Dordrecht.
17. Deierlein G.G., Reinhorn A.M., and Willford M.R. 2010. Nonlinear structural analysis for seismic design. NIST GCR 10-917-5, National Institute of Standards and Technology, Gaithersburg, MD, USA.
18. EERI. 1994. Northridge Earthquake January 17, 1994. Preliminary Reconnaissance Report, Earthquake Engineering Research Institute (EERI), Oakland, CA.
19. El-Metwally S.E. and Chen W.F. 1988. Moment-rotation modeling of reinforced concrete beam-column connections. *Structural Journal* 85(4), 384-394.
20. Elmorsi M., Kianoush M.R. and Tso W.K. 2000. Modeling bond-slip deformations in reinforced concrete beam-column joints. *Canadian Journal of Civil Engineering* 27(3), 490-505.
21. Filippou F.C. and Issa A. 1988. Nonlinear analysis of reinforced concrete frames under cyclic load reversals. *Technical Report*, Report No. UCB/EERC-88/12, EERC, University of California, Berkeley, CA, USA.
22. Fillipou F.C., Popov E.P. and Bertero V.V. 1983. Effects of bond deterioration on hysteretic behaviour of reinforced concrete joints. *Technical Report*, Report No. UCB/EERC-83/19, EERC, University of California, Berkeley, CA, USA.
23. Fragiadakis M., Pinho R. and Antoniou S. 2007. Modeling inelastic buckling of reinforcing bars under earthquake loading. *ECCOMAS Thematic Conference on Computational Methods* 13-16 June, Crete, Greece.
24. Freitas J.A.T., Almeida J.P.M. and Pereira E.M.B.R. 1999. Non-conventional formulations for the finite element method. *Computational Mechanics* 23(5-6), 488-501.
25. Gautam D., Adhikari R. and Rupakhety R. 2021. Seismic fragility of structural and non-structural elements of Nepali RC buildings. *Engineering Structures* 232(),111879.
26. Ibarra L.F., Medina R.A. and Krawinkler H. 2005. Hysteretic models that incorporate strength and stiffness deterioration. *Earthquake Engineering and Structural Dynamics* 34(12), 1489-1511.
27. Mander J.B., Priestley M.J.N. and Park R. 1988. Theoretical stress-strain model for confined concrete. *Journal of Structural Engineering ASCE* 114 (ST8), 1804-1826.
28. Martinez-Rueda J.E. and Elnashai A.S. 1997. Confined concrete model under cyclic load. *Materials and Structures* 30(197), 139-147.
29. Neuenhofer A. and Filippou F.C. 1997. Evaluation of nonlinear frame finite-element models. *Journal of Structural Engineering ASCE* 123(7), 958-966.
30. Ghobarah A. and Biddah A. 1999. Dynamic analysis of reinforced concrete frames including joint shear deformation. *Engineering Structures* 21, 971-987.
31. Hellesland J. and Scordelis A. 1981. Analysis of RC bridge columns under imposed deformations. *IABSE colloquium on Advanced Mechanics of Reinforced Concrete*, Delft, Netherlands, pp 545-559.
32. Khan M.S., Basit A. and Ahmad, N. (2021). A simplified model for inelastic seismic analysis of RC frame have shear hinge in beam-column joints. *Structures* 29(), 771-784.
33. Kunnath S.K., Hoffmann G., Reinhorn A.M. and Mander J.B., 1995. Gravity-load-designed reinforced concrete buildings–Part I: Seismic evaluation of existing construction and Part II: Evaluation of detailing enhancements. *ACI Structural Journal* 92(3), 343-478.
34. Lowes L.N. and Altoontash A. 2003. Modeling reinforced-concrete beam-column joints subjected to cyclic loading. *Journal of Structural Engineering ASCE* 129(12), 1686-1697.
35. Lowes L.N., Mitra N. and Altoontash A.A. (2004). A beam-column joint model for simulating the earthquake response of reinforced concrete frames. *Technical Report*, Report no. PEER 2003/10. Pacific Earthquake Engineering Research Center, University of California, Berkeley, CA, USA.
36. Madas P. 1993. *Advanced Modelling of Composite Frames Subjected to Earthquake Loading*. PhD Thesis, Imperial College London, London, UK.
37. Mari A. and Scordelis A. 1984. Nonlinear geometric material and time dependent analysis of three dimensional reinforced and prestressed concrete frames. *SESM Report 82-12*, Department of Civil Engineering, University of California, Berkeley, CA, USA.
38. Masoudi M., Khajevand S. 2020. Revisiting flexural overstrength in RC beam-and-slab floor systems for seismic design and evaluation. *Bulletin of Earthquake Engineering* 18(11), 5309-534.
39. Menegotto M. and Pinto P.E. 1973. Method of analysis for cyclically loaded R.C. plane frames including changes in geometry and non-elastic behaviour of elements under combined normal force and bending. *Symposium, International Association for Bridge and Structural Engineering*, Zurich, Switzerland, 15-22.
40. Moehle J.P. and Mahin S.A. 1991. Observations on the behavior of reinforced concrete buildings during earthquakes. ACI Special Publication 127, 67-90.

 doi:10.20944/preprints202210.0017.v1

41. Monti G. and Nuti C. 1992. Nonlinear cyclic behavior of reinforcing bars including buckling. *Journal of Structural Engineering,* 118(12), 3268-3284.
42. Monti G., Nuti C. and Santini S. 1996. *CYRUS - Cyclic Response of Upgraded Sections,* Report No. 96-2, University of Chieti, Italy.
43. Ning C.L., Yu B. and Li B. 2016. Beam-column joint model for nonlinear analysis of non-seismically detailed reinforced concrete frame. *Journal of Earthquake Engineering* 20(3), 476-502.
44. Pampanin S., Magenes G. and Carr A. 2003. Modeling of shear hinge mechanism in poorly detailed RC beam-column joints. In: Concrete structures in seismic regions: fib,. *symposium*, May 6-8, Athens, Greece. Paper no; 2003. p. 171.
45. Pampanin, S., Calvi, G.M. and Moratti, M. 2002. Seismic behavior of RC beam-column joints designed for gravity loads. *Proceedings of the 12th European Conference on Earthquake Engineering,* 9-13th September 2002, London, UK. Paper no. 726
46. Papadrakakis M., Charmpis D.C., Lagaros N.D. and Tsompanakis Y. 2008. *Computational structural dynamics and earthquake engineering: structures and infrastructures Vol 2* CRC Press/Balkema, 2300 AK Leiden,The Netherlands.
47. Park, R. 2002. A summary of results of simulated seismic load tests on reinforced concrete beam-column joints, beams and columns with substandard reinforcing details. *Journal of Earthquake Engineering* 6(2), 147-174.
48. Paulay T. and Priestley M.J.N. 1992. *Seismic design of reinforced concrete and masonry buildings*. John Wiley & Sons Inc., NY, USA.
49. Priestley, M.J.N. 1997. Displacement-based seismic assessment of reinforced concrete buildings. *Journal of Earthquake Engineering* 1(1), 157-192.
50. Rizwan M., Ahmad N. and Khan, A.N. 2018. Seismic performance of compliant and noncompliant special moment-resisting reinforced concrete frames. *ACI Structural Journal*, 115 (4), 1063-1073.
51. Sharma A., Eligehausen R. and Reddy G.R. 2011. A new model to simulate joint shear behavior of poorly detailed beam-column connections in RC structures under seismic loads. Part I: Exterior joints. *Engineering Structures* 33(3),1034-51.
52. Shin M. and LaFave J.M. 2004. Testing and modelling for cyclic joint shear deformations in RC beam-column connections. *Proceedings of the 10th World Conference on Earthquake Engineering,* Vancouver, B.C., Canada. Paper no. 0301.
53. Sivaselvan M. and Reinhorn A.M. 1999. *Hysteretic Models for Cyclic Behavior of Deteriorating Inelastic Structures*. Report MCEER-99-0018, MCEER, SUNY at Buffalo, NY, USA.
54. Spacone E., Filippou F.C. and Taucer F. 1996a. Fibre beam-column model for non-linear analysis of R/C frames. *Earthquake Engineering and Structural Dynamics* 25(7), 711-725.
55. Spacone E., Ciampi V. and Filippou F.C. 1996b. Mixed formulation of nonlinear beam finite element. *Computers and Structures* 58(1), 71-83.
56. Taucer F.F., Spacone E. and Filippou, F.C. 1991. A fiber beam-column element for seismic response analysis of reinforced concrete structures. *EERC Report 91/17,* Earthquake Engineering Research Center, University of California, Berkeley, CA.
57. Tsonos A.G. 2007. Cyclic load behaviour of reinforced concrete beam-column subassemblages of modern structures. *ACI Structural Journal* 104(4), 468-78.
58. Vecchio F.J. and Collins M.P. 1986. The modified-compression field theory for reinforced concrete elements subjected to shear. *ACI Journal* 83(2), 219-31.
59. Badrashi, Y.I. 2016. *Response modification factors for reinforced concrete buildings in Pakistan*. PhD Thesis. Department of Civil Engineering, UET Peshawar, 25000 KP, Pakistan.
60. Youssef M. and Ghobarah A. 2001. Modelling of RC beam-column joints and structural walls. *Journal of Earthquake Engineering* 5(1), 93-111.